Earth-Science Reviews 243 (2023) 104472

Contents lists available at ScienceDirect

Earth-Science Reviews

journal homepage: www.elsevier.com/locate/earscirev

Main controlling factors and movability evaluation of continental shale oil

Xiongqi Pang [a,b,*], Min Li [a,b,*], Boyuan Li [a,b,c], Tong Wang [a,b], Shasha Hui [a,b], Yang Liu [a,b], Guoyong Liu [d], Tao Hu [a,b], Tianwu Xu [e], Fujie Jiang [a,b], Hong Pang [a,b], Chenxi Wang [a,b]

[a] State Key Laboratory of Petroleum Resources and Prospecting, China University of Petroleum (Beijing), Beijing 102249, China
[b] College of Geosciences, China University of Petroleum (Beijing), Beijing 102249, China
[c] CNPC Research Institute of Economics and Technology, Beijing 100724, China
[d] Jidong Oilfield Company, PetroChina, Hebei 063004, China
[e] Research Institute of Exploration and Development, Zhongyuan Oilfield Company, SINOPEC, Puyang 457001, China

ARTICLE INFO

Keywords:
Fossil energy
Unconventional oil and gas
Continental shale oil
Shale oil movability
Shale oil recoverable resources

ABSTRACT

Despite the enormous potential of continental shale oil resources, only recoverable shale oil is economically valuable. Shale oil development decisions can greatly benefit from an accurate assessment of recoverable shale oil resources. Three crucial factors for evaluating shale oil recoverable resources are shale oil content, movable oil ratio, and recovery factor. However, because of the significant variety of continental shale, it is challenging to define the aforementioned characteristics. The methodologies and technology for determining the shale oil recoverable resource evaluation parameters, particularly the shale oil content, movable oil ratio, and recovery factor, are thoroughly discussed in this paper. Taking the Tertiary Sha-3 continental shale in Dongpu and Nanpu sags in Bohai Bay Basin, eastern China as an example, the shale oil content was obtained by the pyrolysis method with light and heavy hydrocarbon calibration comprehensively considered, and the main controlling factors of shale oil content were explored. Four geological parameters, including the sedimentary facies, pore structure, surrounding rock quality, and burial depth, primarily regulate the variation features of continental shale oil. The formation mechanism and primary governing variables of movable oil were then revealed using a physical simulation experiment. As porosity and permeability rise, clay mineral content falls, oil viscosity falls, and kerogen concentration rises, the movable oil ratio rises as well. Through stepwise linear regression, a quantitative estimation model for movable oil ratio was developed. After that, a literature search was used to determine the average recovery factor for continental shale oil. Finally, using the volume method model and the Monte Carlo methodology, the recoverable shale oil resources in the Gaoliu area of Nanpu Sag were assessed. The retention, movability, and resource potential of continental shale oil are better understood as a result of this study.

1. Introduction

Shale gas exploration and development have increased on a global scale as a result of the success of the shale gas revolution in the United States. Petroleum geologists' interest in shale oil has gradually grown as a result of the emergence of shale gas. The shale oil refers to the retained liquid hydrocarbons in pore-fracture systems in the organic-rich shale strata, which are characterized by in-situ or extremely short-distance migration and accumulation (Zou et al., 2013a). Therefore, shale oil is also called retained oil. The shale oil reservoir is dense, with matrix permeability $<0.001 \times 10^{-3}$ μm^2 and porosity ranging from 4% to 6%. The shale oil is continuously distributed in a large area in the basin, which is not controlled by geological structure and trap, but by the shale distribution area, and organic matter abundance, type and maturity. Shale oil resources are very considerable on Earth. It's estimated that the recoverable resources of shale oil worldwide are 1501.3×10^8 t (EIA, 2011; IHS Energy, 2014; Zou et al., 2015a). The shale oil resources in the world are widely distributed in >152 marine and continental shale formations in 101 basins (EIA, 2012). Typical representatives of marine shale oil formations include Bakken Formation in the Williston Basin, Eagle ford Formation in the Gulf of Mexico Basin, Wolfcape Formation in the Permian Basin, Woodford Formation in the Anadarko Basin, Marcellus Formation in the Appalachian Basin, and Barnett Formation in the Fort Worth Basin (Altawati et al., 2021; Abrams and Thomas, 2020; French et al., 2020; Hou et al., 2021a; Shao et al., 2020a; Smith, 2018). Foreign continental shale oil is widely distributed in the United States,

* Corresponding authors at: State Key Laboratory of Petroleum Resources and Prospecting, China University of Petroleum (Beijing), Beijing 102249, China.
E-mail addresses: pangxq@cup.edu.cn (X. Pang), liminupcqd@163.com (M. Li).

https://doi.org/10.1016/j.earscirev.2023.104472
Received 20 August 2022; Received in revised form 25 April 2023; Accepted 9 June 2023
Available online 12 June 2023

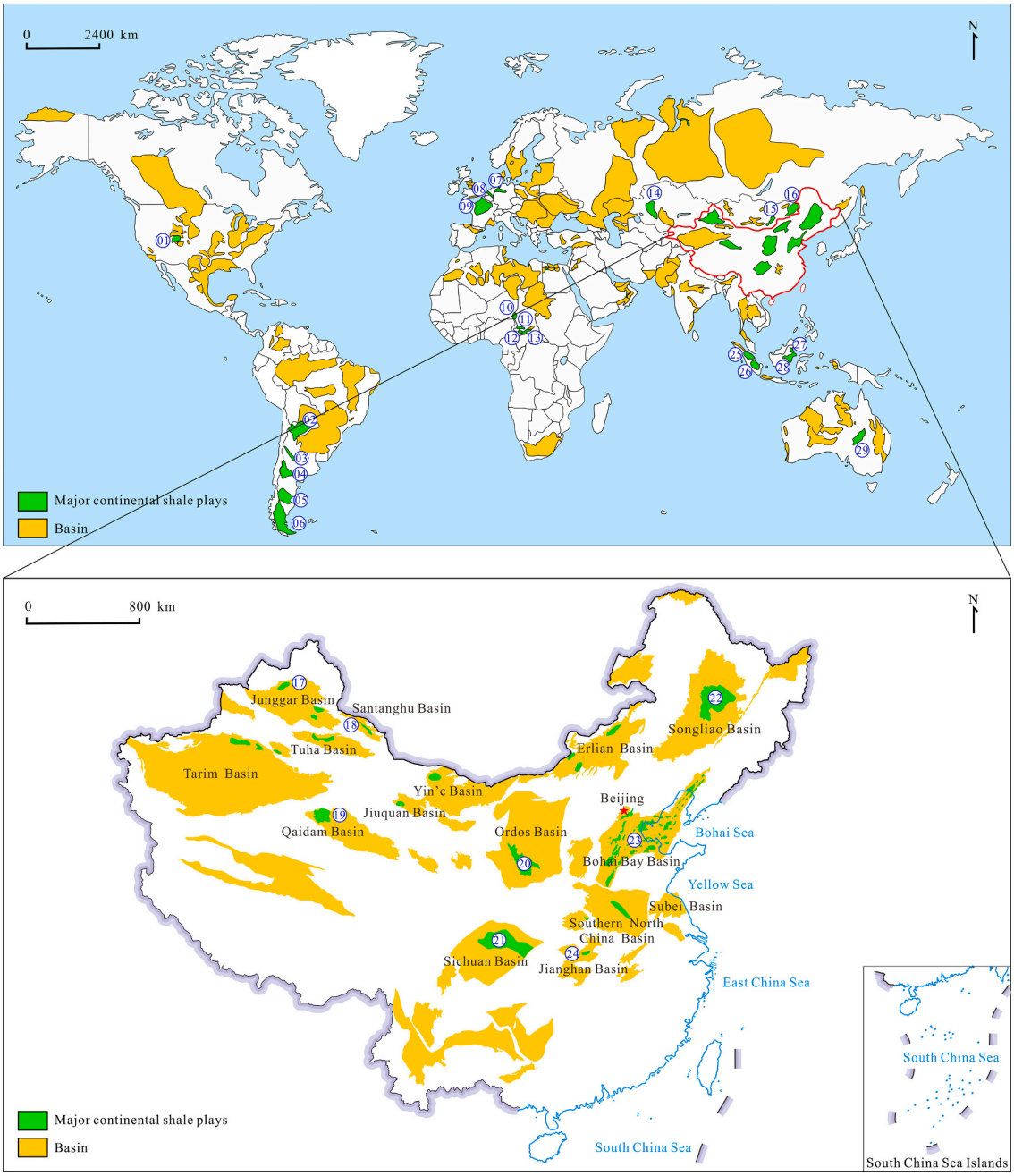

Fig. 1. Distribution of continental shale oil plays in the world (Modified after Li et al. (2022a, 2022b) and Wang et al. (2022c)).

Argentina, Australia, Chad, Indonesia, France, Germany (Supplementary table 1, Fig. 1). When compared to marine shale oil, continental shale oil has a number of distinct properties (Fu et al., 2021;Ma et al., 2022a;Fu et al., 2021; Ma et al., 2022a; Sun et al., 2021; Zhao et al., 2020a). The marine shale oil has the characteristics of high thermal evolution degree (Ro values of 1.0% ~ 1.7%), good parent material type with kerogen of type I, light crude oil density (0.77–0.79 g/cm^3), high gas-oil ratios (50–300 m^3/m^3), large area continuous distribution of strata, and high brittle mineral content. Continental shales, on the other hand, are primarily distinguished by considerable heterogeneity, low to

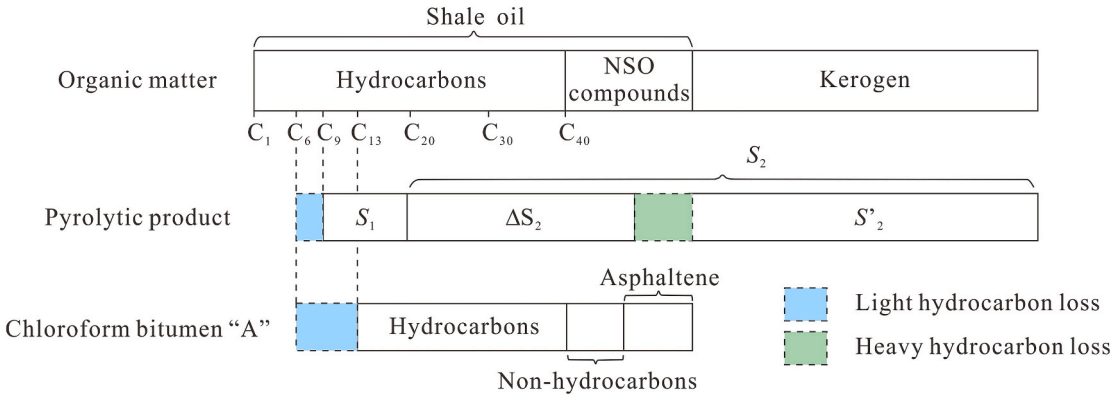

Fig. 2. Comparison of pyrolysis products, chloroform asphalt "A" and shale oil components (Modified after Bordenave (1993)).

medium maturity (Ro values of 0.7% ~ 1.1%), complicated kerogen underlying material type, heavy crude oil density (>0.85 g/cm^3), low gas-oil ratios (20–60 m^3/m^3), and high clay mineral content. Nineteen percent of all shale oil resources are found in the continental United States (EIA, 2012).

Preliminary studies show that China's shale oil resource potential is as high as 200.88 billion tons (Hu et al., 2020). In China, continental shale oil is primarily found in the Permian Lucaogou Formation and Fengcheng Formation in the Junggar Basin, the Triassic Yanchang Formation in the Ordos Basin, the Jurassic Qianfoya Formation and Ziliujing Formation in the Sichuan Basin, the Cretaceous Qingshankou Formation in the Songliao Basin, the Paleogene Shahej (Fig. 1). China's continental shale oil has vast exploration and development opportunities, according to contemporary exploration practice (Zou et al., 2013b). Well AS 1, the first shale oil exploration well in Biyang Sag of Nanxiang Basin, has a maximum daily oil production of 4.68 m^3 after fracturing in a large set of mudstone intervals in He-3 member of Paleogene, making the first breakthrough in continental shale oil in China (Zhang et al., 2019); After fracturing, the Sha-3 shale in well SG 165 in the Liaohe Depression of the Bohai Bay Basin produced 24 m^3 of oil per day, and the Sha-3 shale in well PS 18–1 in the Puyang Depression produced 420 m^3 per day (Wu et al., 2013). Some experts predict that China's annual shale oil production will reach 80 billion to 100 billion tons by 2030 (He, 2017). The issue that the real shale oil production does not match its resource potential is becoming more and more evident with the domestic continental shale oil exploration and development. Petroleum professionals have gradually begun to pay attention to the assessment of movable shale oil resources. There are three states of shale oil: free, bound, and dissolved (Zhu et al., 2021). Free oil typically accumulates in substantial pores and fractures and flows in accordance with Darcy's law (Sun and Zhang, 2020). Bound oil mainly refers to shale oil in the state of adsorption and swelling (Jiang et al., 2016b). Adsorbed oil subjected to van der Waals force is found at the surface of organic matter and minerals as well as in kerogen organic matter. Swelling oil is "embedded" in kerogen. The two lack fluidity and are challenging to be extracted under current technical conditions. Dissolved oil refers to the oil that is dissolved in kerogen, residual water and natural gas, and can be disregarded because of its modest proportions (Zhang et al., 2014; Hu et al., 2021). It should be noted that not all free oils are movable, and free oil that can be effectively exploited under current technical processes, are called movable oil (Zhang et al., 2022). Free oil is theoretically equal to the maximum movable oil (Li et al., 2019a). Thus, the movable oil is the main target of shale oil exploration and production. The movable oil content in shale determines the enrichment degree and production benefit of the shale oil resources (Hu et al., 2021). However, the movability of continental shale oil is influenced by complex factors. The strong heterogeneity of continental shale also causes great difficulties in the study of shale oil movability. As can be seen, the accurate characterization of shale oil movability and clarification of the main controlling factors on shale oil movability are of great significance for the evaluation, prediction and commercial exploitation of movable shale oil and recoverable shale oil resources.

This paper firstly summarizes the determination methods of shale oil content and movable oil ratio, and reviews the main controlling factors on shale oil retention and movability. Then taking the Tertiary Sha-3 continental shale in Dongpu and Nanpu sag in Bohai Bay Basin, eastern China as an example, this study investigates the primary influencing factors of oil retention in shale. A physical simulation experiment was applied to reveal the formation mechanism of movable oil and establish the quantitative relationship between movable oil content and the main controlling factors. Finally, the recoverable shale oil resources were evaluated.

2. Review of evaluation methods and main controlling factors of shale oil

2.1. Evaluation of shale oil content

The shale oil content refers to the oil amount per unit weight of shale, and a key parameter to calculate shale oil resources by volume method. The commonly used oil content parameter is the corrected pyrolytic hydrocarbon S_1 or chloroform bitumen "A".

2.1.1. Pyrolytic parameter S_1

The pyrolysis parameter S_1 was obtained by demonstrating Rock-Eval pyrolysis experiment. S_1 refers to the content of hydrocarbon products that evaporated before 300 °C during the heating process of pyrolysis experiment and have existed in the source rock, which is the content of free hydrocarbon (mg/g). However, some heavy hydrocarbon products that have been present in mud shale have boiling points that are significantly higher than 300 °C, therefore the remaining hydrocarbons in the shale cannot be thermally evaporated entirely before this temperature. As a result, after 300 °C, certain remaining hydrocarbons can only be recognised as S_2. Additionally, the gas hydrocarbon (C_{1-5}) and light liquid hydrocarbon (C_{6-9}) in shale have been lost during the core's journey from the well's bottom to the surface, its extended storage in the core library, and the sample's crushing prior to the experiment (Xue et al., 2015). It can be seen that S_1 cannot completely represent the retained oil in shale, and shale oil should include the following three parts: (1) measured S_1; (2) small molecular hydrocarbons that have been lost before pyrolysis analysis; (3) heavy residual hydrocarbons detected as S_2 (Fig. 2). Therefore, light hydrocarbon compensation and heavy hydrocarbon correction are required for pyrolysis parameter S_1.

Wang and Zheng (1987) performed pyrolysis chromatographic analysis experiments on core samples of oil-generating rocks of different maturities in various basins to correct the heavy hydrocarbon content of S_1. They discovered that S_2 contained specific heavy hydrocarbon

components ($C_{33–40}$), and various source rock types had different contents of heavy hydrocarbon components at various stages of evolution. They calculated correction coefficients of heavy hydrocarbon for various types of source rocks based on the experimental data. Xue et al. (2015) took the difference of pyrolysis parameters S_2 and S_2' of shale samples before and after the extraction of chloroform asphalt "A" as the heavy hydrocarbon loss content ($\Delta S = S_2 - S_2'$), and the ratio of ΔS to S_1 represents the heavy hydrocarbon recovery coefficient of S_1. By contrasting the outcomes of the multi-temperature pyrolysis experiment with the findings of the traditional pyrolysis experiment, Xu et al. (2021) were able to calculate the heavy hydrocarbon correction coefficient of S_1. Different scholars have also proposed many methods for light hydrocarbon correction of S_1. Michael et al. (2013) calculated the loss of light hydrocarbons using the link between crude oil density index (API) and low boiling point component (C_{15-}) content. Chen et al. (2018a) developed a calculation model based on the material balance theory to assess the loss of light hydrocarbons using parameters like S_1, S_2, the maximum pyrolysis peak temperature Tmax from Rock-Eval pyrolysis, and TOC content from the organic carbon test. Zhu et al. (2015) used a comparative experimental approach to conduct rapid pyrolysis of samples under liquid nitrogen freezing and conventional pyrolysis of samples after 30 days of room temperature storage, respectively. The amount of light hydrocarbon loss was determined by the difference between the two groups of experiments' hydrocarbon generation potentials. Zhao et al. (2021a) carried out several groups of controlled experiments: (1) They put the frozen samples at room temperature for 24 h, 48 h and 72 h respectively, and then conducted pyrolysis analysis on these samples; (2) They grounded the samples in the closed system and the open system at room temperature respectively, and then conducted pyrolysis analysis these samples; (3) They compared the results of conventional pyrolysis and multi-stage pyrolysis. Finally, they estimated the recovery coefficient of light hydrocarbon by analyzing the hydrocarbon loss rates of the above experiments. Chen et al. (2019) used the gas-to-oil ratio of the dissolved gas or the formation volume factor to calculate the content of light hydrocarbon loss based on the principle of phase equilibrium and pyrolysis light hydrocarbon loss under various temperature and pressure settings. But only source rock samples from the oil generation window can be used with this technique.

2.1.2. Chloroform asphalt "A"

The content of chloroform asphalt "A" was obtained by chloroform extraction. Chloroform bitumen "A" and shale oil have several chemical components, including petroleum hydrocarbons and NSO compounds. (Fig. 2). The chloroform extraction method operates on the following principles: Crushed rock samples are placed into a paper cylinder that was placed into the extractor's sample chamber; the sample is then extracted with chloroform until the extraction solution's fluorescence falls below level 3; Transfer the extract solution to the weighing bottle to evaporate and dry; Measure the weight difference between the empty weighing bottle and the weighing bottle containing the chloroform asphalt to determine the mass of the chloroform asphalt "A" (Xue et al., 2015). The light hydrocarbon portion of $C_{6–13}$ with strong movability in shale oil volatilizes out as a result of the chloroform extraction process's phase of volatilizing chloroform. Therefore, it is necessary to correct the content of chloroform asphalt "A" with light hydrocarbon. Based on the similarity between the components of crude oil in self-generated and self-stored reservoir and the retained liquid hydrocarbon in shale, Zhu et al. (2015) used the analogy method to calculate the proportion of light hydrocarbon loss in the chloroform extraction process in order to establish the correction model of light hydrocarbon in chloroform asphalt "A" during hydrocarbon generation evolution. According to the chemical kinetics principle, Xue et al. (2015) calibrated the chemical kinetics of the primary pyrolysis of kerogen and the secondary pyrolysis of crude oil. They then obtained the chemical kinetics parameters of each reaction and used the Easy-Ro model to calculate the yield ratio of each oil and gas component ($C_{6–13}$, C_{13+}) corresponding to various Ro.

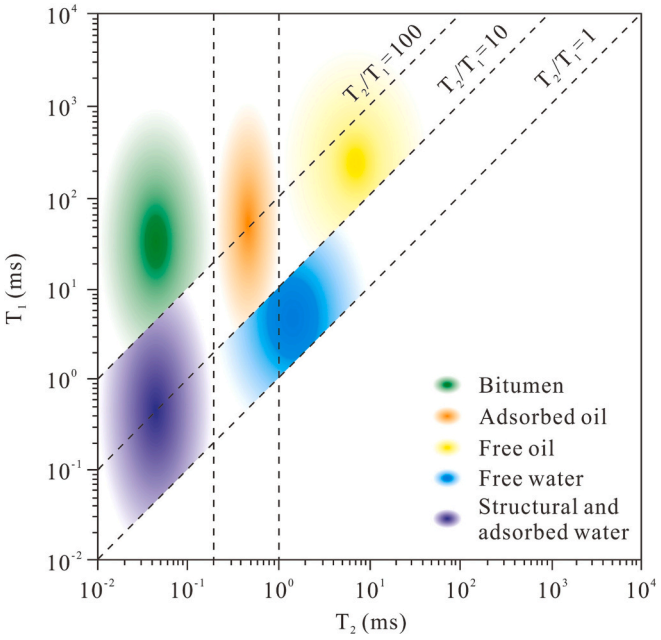

Fig. 3. The T_1-T_2 map identifying different fluid components (Modified after Li et al., 2020, Ma et al. (2022b), Xu et al. (2022)).

Then, the chloroform asphalt "A" light hydrocarbon correction coefficient corresponding to various Ro is determined. This approach, however, only takes into account light hydrocarbons with organic maturity larger than 0.8%.

2.2. Evaluation of movable oil content

For shale oil exploration and development, it is necessary to evaluate not only the total amount of retained oil in shale formations but also how much of retained oil is movable (Li, 2014; Wang et al., 2022a). Therefore, the main focus of the shale oil resource evaluation is to ascertain the movable oil ratio in the rock. The quantitative characterization of movable oil in marine shale has significantly advanced in recent years. For analyzing the quantity and ratio of movable oil in shale, predecessors primarily established five techniques.

2.2.1. Oil saturation index method

The oil saturation index method uses OSI (OSI=S_1/TOC × 100) to evaluate shale oil movability, and the OSI value of 100 HC/g TOC is taken as the lower limit for oil effective flow (Pepper and Corvi, 1995; Lopatin et al., 2003; Jarvie, 2012; Jarvie and Daniel, 2012). The higher the OSI value, the better the movability. The oil saturation index method is a simple and convenient method to evaluate shale oil movability. However, this method is not applicable to the movability evaluation of continental shale oil with strong heterogeneity due to its single factor. The OSI is relative value, even if it is large (> 100), the oil content in reservoir is not large for shale with low TOC (< 1.0%), the OSI cannot reflect oil product information. is not a reliable indicator for all shale formations. Not all shale reservoirs of different types can use OSI = 100 as the dividing line of high-quality reservoirs.

2.2.2. Nuclear magnetic resonance (NMR) and centrifugal/displacement analysis

The combination of Nuclear Magnetic Resonance (NMR) and centrifugal/displacement analysis has been proved to be a good application to evaluation of shale oil movability (Li, 2014; Lu, 2017). The principle of this method is to conduct NMR analysis before and after displacement or centrifugation of oil-saturated core (coexistence of free and adsorbed state), and evaluate the content, proportion and distribution

characteristics of movable oil in core by NMR T_2 spectra. Furthermore, the microscopic occurrence states (adsorbed or free) of pore fluid can be indicated by two-dimensional NMR (T_1-T_2) (Fleury and Romero-Sarmiento, 2016; Zhang et al., 2022). T_1/T_2 can reflect the interaction strength between fluid and shale matrix, so as to identify the occurrence state of shale oil (Khatibi et al., 2019; Ma et al., 2020)。As displayed by Fig. 3, five significant regions of different fluid components are defined: (1) bitumen with T_1 value >10 ms and T_2 value <0.2 ms, (2) movable oil with T_1 value >10 ms, 1 ms < T_2 value <100 ms, and T_1/T_2 value >10, (3) adsorbed oil with T_1 value >2 ms, 0.2 ms < T_2 value <1 ms, and T_1/T_2 value >2, (4) structural and adsorbed water with T_1 value <10 ms, T_2 value <0.2 ms, and 1 < T_1/T_2 value <100, and (5) free water with T_1 value <10 ms, T_2 value >0.2 ms. Two points should be paid attention to when using this method. First, the speed of centrifugation will affect the experimental results. Zhu et al. (2021) studied the variation characteristics of movable fluid content at four centrifugal speeds which are 3000, 6000, 9000, and 12,000 r/min, and found that the higher the centrifugal speed, the higher the movable fluid content. It remained impossible, however, to determine whether the centrifugal force was sufficient to remove all the movable oil in the cores during the laboratory centrifugation analyses (Zhang et al., 2022). Li et al. (2019a) has established a relationship between centrifugal force and movable oil content to determine the maximum movable oil content. In addition, due to the low porosity and permeability of shale samples, excessive pressure may lead to shale fracture, affecting the accuracy of experimental results.

2.2.3. Gradual pyrolysis/heating release method

The gradual pyrolysis/heating release method is an improvement on the traditional pyrolysis method (Li et al., 2016). The traditional heating procedure consists of two temperature stages. The first temperature stage is 300 °C constant temperature, and the pyrolysis hydrocarbon analysis of rock is carried out to obtain the S_1 peak, which is the soluble hydrocarbon in the samples. The second is heated to 650 °C at a constant rate to obtain S_2 peak, which is the residual hydrocarbon generation potential of the sample organic matter. However, studies have shown that pyrolysis S_1 is not all free oil, and pyrolysis S_2 contains both a small amount of free oil and adsorbed oil (Wang et al., 2019a). In order to overcome the shortcomings of traditional pyrolysis methods, predecessors have proposed the multi-temperature pyrolysis method. The principle of this method is that shale oil in different occurrence states has different thermal volatilization capacity due to its different molecular composition. Therefore, shale oil in different occurrence states can be quantitatively characterized by reasonably setting the heating experimental conditions in the pyrolysis process. This method has strict requirements on experimental conditions. Taking the multi-temperature pyrolysis experimental method proposed by Jiang et al. (2016b) as an example, the specific operation process is as follows: powder shale samples are kept at 200 °C for 1 min to detect the product S_{1-1}, and then heated to 350 °C at a rate of 25 °C/min and kept constant temperature for 1 min to detect the product S_{1-2}. When the temperature exceeded 350 °C, it was heated to 450 °C at a rate of 25 °C/ min and kept constant for 1 min to detect the product S_{2-1}. After the temperature reached 450 °C, it was heated to 600 °C at a rate of 25 °C/min to detect product S_{2-2}. S_{1-1}, ($S_{1-1} + S_{1-2}$), S_{2-1} and S_{2-2} represent the content of actual movable oil, maximum movable oil, adsorbed oil and kerogen cracking oil, respectively. However, a large amount of light hydrocarbon loss will occur during core preservation and sample preparation(Lafargue et al., 1998; Behar et al., 2001), resulting in the evaluation results accuracy of movable oil content, and light hydrocarbon correction must be carried out.

2.2.4. Solvent step extraction method

The solvent step extraction method (Ritter, 2003; Ertas et al., 2006; Li et al., 2017) gradually extracts free oil with less polarity and adsorbed oil with more polarity by using different solvents based on the different molecular polarities of shale oil in different occurrence states, and then quantitatively characterizes them respectively. Song et al. (2005) used chloroform, methanol-acetone-chloroform terpolymer solvent and carbon disulfide - (*N*-methyl-2-pyrrolidone) mixed solvent to extract free oil and adsorbed oil and determine its content step by step. Qian et al. (2017) successively extracted rock samples with a weak polar solvent (dichloromethane/methanol volume ratio of 93:7) and a strong polar solvent (tetrahydrofuran/acetone/methanol volume ratio of 50:25:25), and quantitatively analyzed the extracted products, so as to obtain the content and proportion of free oil. This method's operation is complex, and the extraction procedure may alter the material's surface's wettability. Additionally, shale oil may dynamically change in different occurrence states, which could have an impact on the accuracy of experimental results.

Table 1
Statistical results of movable oil ratios in the world.

Country	Sedimentary environment	Research area or horizon	Movable oil ratio (%)	Data source
America	Marine	Barnett Shale	13.54–89.11 (mean 29.36)	(Han et al., 2015)
Germany	Lacustrine	Wealden Shale, Lower Saxony Basin	4.2–16.63 (mean 9.4)	(Zink et al., 2016)
Germany	Marine	Posidonia Shale	>10.0	(Ziegs et al., 2017)
Argentine	Marine	Vaca Muerta Shale	>30.0	
China	Lacustrine	Lucaogou Formation, Junggar Basin	17.30–69.28 (mean 48.15)	(Cao et al., 2017)
China	Lacustrine	Qianjiang Formation, Qianjiang Basin	7.12–91.29 (mean 29.31)	(Chen et al., 2018b)
China	Lacustrine	Jiyang Depression, Bohai Bay Basin	3.06–16.25 (mean 8.16)	(Sang et al., 2017)
China	Lacustrine	Shahejie Formation, Dongying depression, Bohai Bay Basin	25.33–97.57 (mean 60.37)	(Li et al., 2018)
China	Lacustrine	4th section of Shahejie Formation, Dongying Depression, Bohai Bay Basin	24.3–24.7	(Li, 2014)
China	Lacustrine	3rd section of Shahejie Formation, Bohai Bay Basin	8–28	(Zhang et al., 2014)
China	Lacustrine	4th section of Shahejie Formation, Bohai Bay Basin	9–30	
China	Lacustrine	Lucaogou Formation, Jimusar Depression, Junggar Basin	5–30	(Jin et al., 2021)
China	Lacustrine	Chang 7_3 section of Yanchang Formation, Longdong area, Ordos Basin	15–30	
China	Lacustrine	2nd section of Kongdian Formation, Cangdong Depression, Bohai Bay Basin	2–10	
China	Lacustrine	1st section of Qingshankou Formation, Changling Depression, Songliao Basin	20–25	

2.2.5. Molecular dynamics simulation method

The molecular dynamics simulation method is a computer simulation technique (Fathi and Akkutlu, 2012; Mosher et al., 2013). It that can simulate the density distribution of oil on various mineral surfaces under various temperature and pressure conditions, as well as on cracks of varying sizes. Based on these calculations, the adsorption and free state content of crude oil components are then calculated, and the movability of shale oil is then estimated (Falk et al., 2015; Tian et al., 2018). According to Wang et al., 2015a, alkane molecules are dispersed on the pore surface in many layers, with densities of the adsorption layers ranging from 1.9 to 2.7 times that of free oil and dropping off quickly from the first to the third layer. Zeng et al. (2023) studied the influence of shale wettability on the relative content of adsorbed oil and free oil by adjusting and modifying the ratio of methyl and hydroxyl groups on quartz surface and changing the wetting angle of quartz surface. The findings demonstrated that when the wetting angle dropped, the amount of free oil progressively increased and the amount of adsorbed oil gradually reduced. However, variables like the simulation parameter settings and model veracity have an impact on how accurate the results of molecular dynamics simulations are.

2.2.6. Statistics of movable oil ratio

Table 1 displays the statistical results of the global and domestic typical shale oil movability ratios. Han et al. (2015) determined that the movable oil ratio of Barnett Shale ranges from 13.54% to 89.11%, with an average of 29.36%, using a large variety of petrological and high-resolution organic geochemical investigations along with the Rock-Eval technique and Soxhlet extraction. According to Zink et al. (2016), the Wealden Shale in the Lower Saxony Basin has a movable oil ratio that ranges from 4.2% to 16.63%, with an average of 9.4% using the Rock-Eval technique. Numerous researchers have used various techniques to look into the movability of shale oil in the Bohai Bay Basin. Sang et al. (2017) used nuclear magnetic resonance (NMR) technology and high-speed centrifugal experiment to compute the movable oil ratio of shale oil reservoir in Jiyang Depression is between 3.06% and 16.25%, with an average of 8.16%. By combining simulation experiment and nuclear magnetic resonance (NMR) analysis, which demonstrated good fluidity, Li (2014) found that the movable oil ratio in the fourth member of the Shahejie Formation in Dongying Sag is between 24.3% and 24.7%. According to calculations by Zhang et al. (2014), the movable oil rates of shales in the third and fourth members of the Shajie Formation in Dongying Sag are in the ranges of 8%–28% and 9%–30%, respectively. These rates were calculated based on the elastic mechanical properties of shale rock and the properties of fluid in shale from the perspective of formation energy. Li et al. (2018) calculated that the movable oil ratio in Shahejie Formation of Dongying Sag is between 25.33% and 97.57%, with an average of 60.37%, using the traditional Rock-Eval approach. According to Cao et al. (2017)'s analysis of the movability of shale oil in the Junggar Basin, the movable oil ratio in the Jimusar Sag's Lucaogou Formation ranges from 17.3% to 69.28%, with an average of 48.15% using Rock-Eval findings. Jin et al. (2021) used electron beam charge effect and adjusted imaging parameters to make the distribution of crude oil show charge effect, so as to obtain the distribution of movable oil. Combined with pyrolysis parameters such as free hydrocarbon content, He calculated that the movable oil ratio in Lucaogou Formation of Jimusar Sag is between 5% and 30%. The movable oil ratios of key shale oil reservoirs in China are between 15% and 30%, 2% and 10%, 10% and 25%, respectively, in the Chang 7_3 submember of Yanchang Formation in the Longdong area of Ordos Basin, the second member of Kongdian Formation in Cangdong Sag of Bohai Bay Basin and the first member of Qingshankou Formation in Changling sag of Songliao Basin. In conclusion, shale oil has a significantly varied movable ratio, often ranging between 10% and 50%, with an average of 25%.

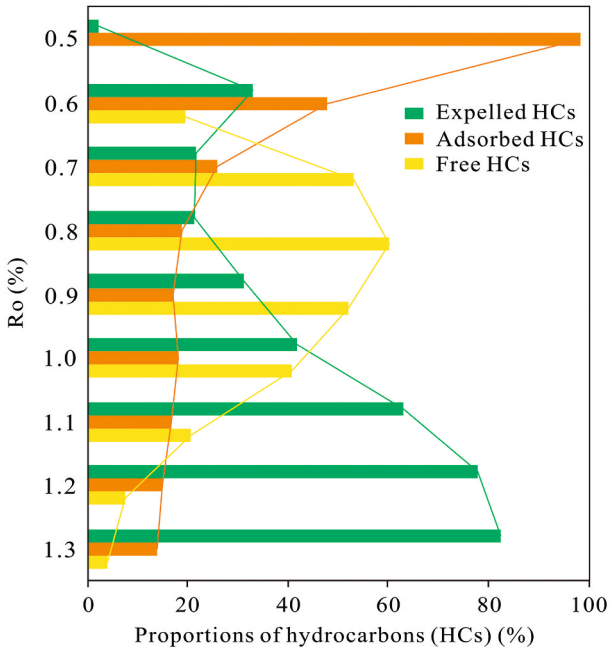

Fig. 4. The proportions of adsorbed hydrocarbon, free hydrocarbon and expelled hydrocarbon with maturity (Modified after Zhao et al. (2020b)).

2.3. Influencing factors of shale oil retention and movability

2.3.1. Organic matter type, abundance and maturity

The type of organic matter in shale regulates both the proportion of free/movable oil as well as the content of residual oil. According to research, type I kerogen produces oil at a rate that is 10 times or even more than type II kerogen, while type II kerogen produces oil at a rate that is 2–7 times higher than type III kerogen. (Zhang et al., 2012). As a result, under the same circumstances, shale with type I and II kerogen has a significant potential for the production of hydrocarbons, which is advantageous for the production and enrichment of shale oil. The abundance of organic matter is also an important factor affecting shale oil content, free oil content and adsorbed oil content. The association between shale oil, free oil, adsorbed oil content, and TOC content was examined by Xu et al. (2022), and they discovered a positive correlation between them. With an increase in TOC content, the proportion of adsorbed oil gradually rises while the percentage of free oil declines because the increase in adsorbed oil content is greater than the increase in free oil content. This tendency is most likely caused by the emergence of more organic pores with larger surface areas as TOC concentration rises, which increases the availability of occurrence sites for adsorbed oil.

Furthermore, numerous prior investigations have shown that the thermal maturity significantly affects the amount of shale oil present and its movability (Wang et al., 2022b;; Zhang et al., 2019). Zhao et al. (2020b) quantitatively assessed the amounts of adsorbed hydrocarbon, free hydrocarbon, and expelled hydrocarbon in different thermal evolution stages of lacustrine shale using thermal simulation and kerogen swelling experiment (Fig. 4). The free hydrocarbon content is at its maximum, accounting for >40% of the total hydrocarbon generation, when the Ro value is 0.7% ~ 1.0%. Guan et al. (2022) observed that the shale oil content and movable oil content increased and then decreased with enhanced maturity in the lacustrine shale of the Funing Formation in the Subei Basin. By influencing the hydrocarbon content and shale pore structure, maturity controls the amount of free oil (Xu et al., 2022). Shale oil first appears in an adsorbed state within or on the surface of organic matter during the early stage of thermal evolution (Ro > 0.5%) (Bagri et al., 2010). After that, the shale oil moves gradually into nearby

pores to create isolated distributions of free oil. As Ro rises, organic pores form, dissolved pores are produced by released organic acid, and the recrystallization effect is thus readily apparent. The shale oil gradually distributed as a continuous free-state into nearby recrystallization intercrystalline pores and structural cracks (Liang et al., 2022). In the late stage of thermal evolution (Ro > 1.3%), the oil pyrolyzed from kerogen contains plentiful saturated hydrocarbon; meanwhile, the heavy oil pyrolyzes and generates light oil (Castro et al., 1998; Liang et al., 2022). Hence, the percentage of the free oil decreases during this stage.

2.3.2. Mineral composition

The influence of mineral components on shale oil content and occurrence state is mainly reflected in the occurrence space and adsorption capacity. Shale is mostly composed of the quartz, clay, carbonate, and pyrite minerals. These inorganic minerals' pores can offer a significant occurrence site for shale oil (Slatt and O'Brien, 2011). Additionally, inorganic minerals have the ability to adsorb shale oil, however this ability is smaller than that of organic matter (Dong et al., 2022). The adsorption capacity of clay minerals is higher than that of other non-clay minerals among inorganic minerals. On the one hand, clay minerals accommodate more adsorption sites for shale oil since their pore surface area is significantly greater than that of non-clay minerals (Passey et al., 2010; Zheng et al., 2018). On the other hand, Al^{3+} and Si^{4+} are frequently replaced by their isomorphism in clay mineral crystals, making the minerals negatively charged and attracting cations like Na^{+}, Ca^{2+}, and K^{+}. These cations increase the ability of clay minerals to absorb electronegative organic macromolecules. (Xu et al., 2022). Consequently, clay minerals typically result in higher enrichment but reduced movability of hydrocarbons over their surface due to their much greater specific surface area than ordinary brittle minerals (Wang et al., 2016). This viewpoint was also supported by Ma et al. (2022b). They discovered that the movable oil contents positively correlate with quartz contents while the association between the movable oil contents and total clay mineral is negative while analyzing the oil-bearing property of lacustrine shale in Qikou Sag Shahejie Formation in the Bohai Bay Basin. It is evident that the proportion of adsorbed oil increases with clay mineral content while the fraction of movable oil decreases.

2.3.3. Pore structure

The pore structure of shale has an influence on the content of free/movable oil and shale oil. Shale oil does not exist in the entire porosity of shale matrix due to its large molecular dimension. To accurately evaluate the predominant pore size of shale oil, it is advised to combine the solvent extraction and fluid injection methods. Li et al. (2015) examined the oil content controlled by various grades of pores in Songliao Basin's Qingshankou Formation shale and discovered that pores larger than 20 nm in diameter (30% of total pore volume) had a better correlation between specific pore volume and oil content, suggesting that shale oil is primarily found in these pores. Su et al. (2018) observed that the pore volume increased most significantly in the range of 3–50 nm aperture by comparing the pore structure parameters before and after trichloromethane extraction. Wang et al. (2019a) compared the pore size distribution characteristics of shale in Shahejie formation of Jiyang depression before and after chloroform extraction, and believed that shale oil was mainly stored in pores with a pore size of 3–80 nm. These findings imply that the primary occurrence spaces of shale oil are mesopores and macropores. Additionally, the pores that store absorbed oil and free oil have different diameters. A crucial technique for determining the pore size related to free oil and adsorbed oil is molecular simulation (Zhong et al., 2013; Zhang et al., 2020). The current molecular simulation can only model shale oil with simple alkane components and uses graphite or single mineral to substitute the shale components, but it can still reflect occurrence law of shale oil (Wang et al., 2015c). By contrasting the mass density profiles within the organic pores of various sizes, Wang et al. (2015b) distinguished between the free oil and adsorbed oil by simulating alkane adsorption on graphite slits. The findings demonstrate that shale oil is adsorbed on graphite wall in several layers, with the number of layers increasing with increasing

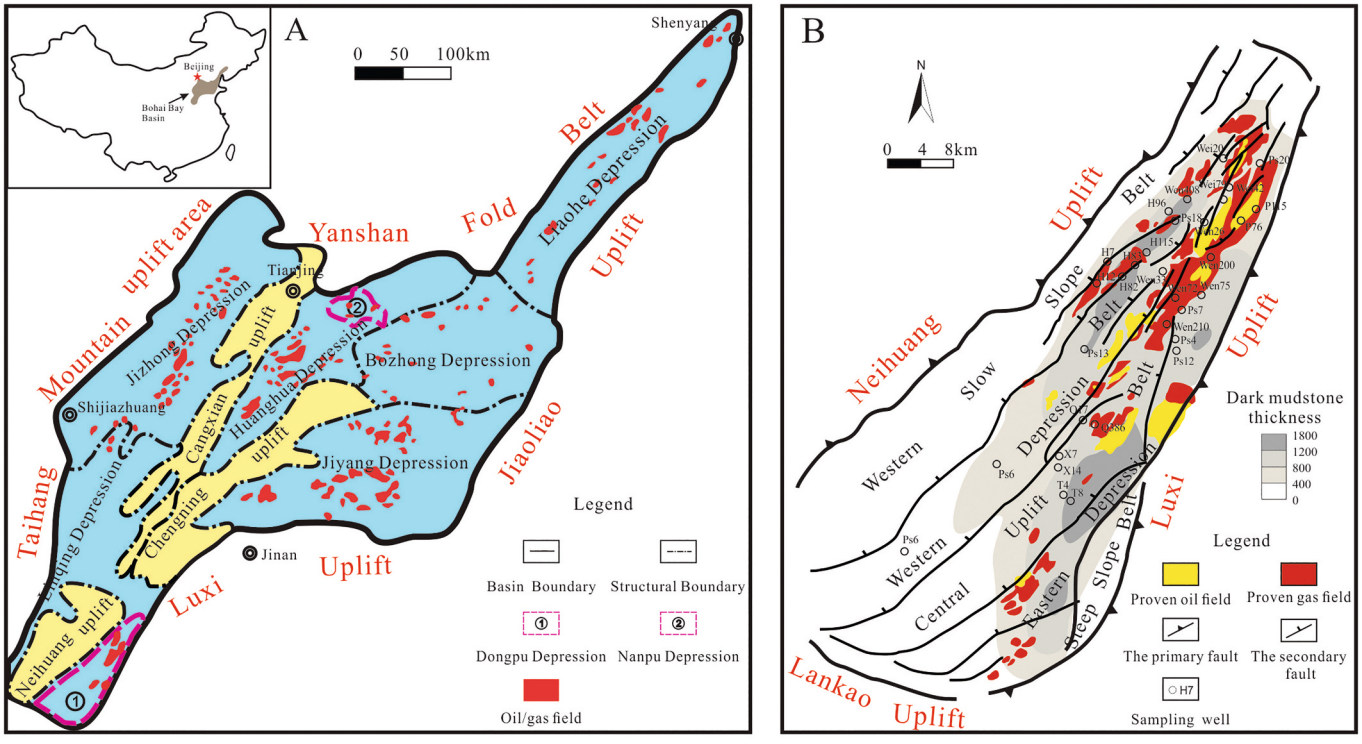

Fig. 5. Oil and gas exploration in Bohai Bay Basin, China, and geographical location of key research areas. A- Oil and gas exploration situation in Bohai Bay Basin and the location of key research areas; B- Tectonic zoning and distribution of Tertiary shale in Dongpu Sag, Bohai Bay Basin.

pore size until it eventually becomes constant. The results also demonstrate that the cut-off pore diameter of the free oil is 3.84 nm in organic pores. The adsorption behavior of oil mixture molecules of eight components contained in graphite and quartz slit-shaped nanopores at 356 K and 18 MPa was simulated by Tian et al. (2017). It was discovered that the critical pore sizes for free oil in the slits of graphite and quartz are, respectively, 3.36 nm and 0.88 nm. According to the previous research, the amount of adsorbed oil and free oil grows along with pore size and pore volume, while the proportion of adsorbed oil falls and the proportion of free oil rises (Wang et al., 2019a). Han et al. (2021) compared the proportion of movable oil in shale with diverse pore throat development characteristics: The movable oil accounted for 46.7% in shale with development of big pore throat (with average pore and throat radius of 187 nm and 168 nm, respectively); Shale with a relatively developed big pore throat (with average pore and throat radius of 102 nm and 66 nm) contains 15.6% of movable oil; However, shale with tiny pore throats contains 8.7% of movable oil (the average pore and throat radius are 87 nm and 58 nm, respectively). It is clear that the movable oil content is significantly influenced by the size of the pores. Moreover, Zhang et al. (2022) discovered a positive correlation between the movable oil content and the pore fractal dimension of lacustrine shale in the Dongying depression. This finding suggests that the proportion of movable oil decreases as pore complexity increases.

2.3.4. Fluid properties

The properties of shale oil, such as the crude oil content, phase state, and viscosity, have an impact on its movability as well. Normally, higher gas-oil ratio (GOR $> 178\ m^3/m^3$) can increase the movability of shale oil (Jarvie, 2014). Moreover, a negative correlation between GOR and viscosity illustrated that the influence of viscosity on shale oil movability is opposite to that of GOR (Hemmati-Sarapardeh et al., 2013). It demonstrates that shale oil movability is not facilitated by high viscosity. Based on both laboratory simulations and observations of sedimentary basins, these properties of shale oil are closely related to shale maturity and change regularly with the thermal evolution of shale. Previous research has employed hydrocarbon generation and expulsion simulation experiments to examine how the composition and properties of hydrocarbon fluids vary throughout thermal evolution and how this affects the shale oil movability. According to the results of the thermal simulation of the hydrocarbon generation and expulsion of Paleogene low mature shale, Bao et al. (2016) hypothesized that during the process of hydrocarbon generation of lacustrine shale, the phase state of hydrocarbon fluid gradually changed from oil to condensate gas, the GOR gradually increased, the viscosity of crude oil in shale decreased significantly, and the shale oil movability gradually increased. Similar research by Hou et al. (2021b) on Permian Lucaogou shales in the Jimusar sag, Junggar Basin, demonstrated that the GOR in shale increased quickly with maturities. On the one hand, during the thermal evolution, cracking of the oil results in an increase in the light components, a gradual increase in the gas amount and GOR, and a decrease in the oil viscosity; On the other hand, increasing burial depth results in increased pressure that improves gaseous hydrocarbon solubility in the share oil, leading to decreased viscosity and enhanced movability of shale oil (Bao et al., 2016).

3. Key study area selection and regional geological survey

The Bohai Bay Basin (Fig. 5A) is selected as the focus of this paper for five main reasons. First, the proven oil and gas reserves are large, and the remaining resource potential is enormous. Secondly, abundant shale oil resources have been found in Tertiary source rocks. Thirdly, many research results and data have been accumulated after years of exploration (Hou, 2014; Cheng and Chen, 2015; Xu and Ji, 2015). Fourthly, many independent fault depressions are developed in the basin with similar geological and reservoir forming conditions (Tao et al., 2022; Zheng et al., 2022). It is beneficial to understand the whole basin by studying a single fault depression. Fifth, the evolution history of the basin is simple (Xia et al., 2022). Nanpu Sag is in the central part of Bohai Bay Basin, at the southern edge of the Yanshantai fold belt in the northeast corner of the Huanghua Depression (Zhu et al., 2013). Dongpu Sag is in the southwest of Linqing Depression in the south part of Bohai Bay Basin, an independent fault depression extending NNE and wide in the south and narrow in the north (Fig. 5B). In this study, the Sha-3 member of Tertiary Shahejie Formation in Nanpu Sag and Dongpu Sag is the key analysis object. The research results and new understanding are used to predict and evaluate the distribution of movable oil sweet spots in the shale.

4. Samples and methods

4.1. Samples

Shale samples were obtained from Sha-3 member of exploration wells in Dongpu Sag and Nanpu Sag, Bohai Bay Basin. The shale samples of Dongpu depression were collected from 16 wells, including Hu7–18, Hu 12–20, Hu82, Hu83, Hu96, Wen26, Wen75, Wen200–6, Wen210, Wei20, Wei42, Wei79–1, PS4, PS6, PS12, and PS18, with depth range of 1777–5194 m. These samples are typical saline-lacustrine shale, containing organic-rich and organic-poor laminae frequently interbedded. Shale samples of Nanpu depression were collected from 10 wells, including G19–10, L68X1, G80–12, G83–10, G18, G3101, L22, G65–1, G5, and G23, in the Gaoliu area of Nanpu Sag, in the range of 2928–4047 m. The shale samples are relatively dense, with common laminar structure developed. Parallel or angular microcracks are common in these samples.

4.2. Routine experimental tests

The total organic carbon (TOC) content was measured by a LECO CS600 carbon sulfur analyzer, referring to Jiang et al. (2016a). Rock pyrolysis experiments were performed on a Rock-Eval VI instrument. During the heating process, pyrolysis parameters of free hydrocarbons (S_1) and potential hydrocarbons (S_2) were obtained when heated to 350 °C and 600 °C, respectively.

Mineral compositions were determined by X-ray diffraction (XRD), which was performed on a D/max- 2500 diffractometer. The mineral content was semi-quantitatively analyzed based on the difference of diffraction patterns of different minerals. Thin sections were observed by a Leica DMLP microscope identify rock mineralogy and bedding structure characteristics of lacustrine shale samples. The slice shale samples polished by Ar ions were observed by a field emission scanning electron microscope (FE-SEM) and the pore morphology, size and type of shale were analyzed. The detailed procedure of the above three experiments can be referred to Wang et al. (2019b), Zhu et al. (2019), and Hu et al. (2019), respectively.

A total of 9 samples of different lithology with good oil-bearing property were selected, and the N_2 adsorption desorption experiment was carried out on the shale samples before and after being extraction with dichloromethane. Shale samples of 5 g weigh were broken into particles with a diameter of 3–4 mm, and then were degasified in vacuum at 110 °C for about 14 h. Nitrogen isothermal adsorption curves were obtained by a Micromeritics ASAP2420 automatic specific surface area (SSA) and pore diameter analyzer. The Brunauer Emmett Teller (BET) model is used to calculate the SSA, and the Barrett Johner Halenda (BJH) model is used to calculate the pore volume and pore size distribution.

4.3. Physical simulation experiments on shale oil movability

4.3.1. Principle of the simulation experiment

This study focuses on simulating the variation characteristics of movable oil ratio in rock media with different porosity, permeability,

Fig. 6. Physical simulation experiment equipment for artificial core preparation and obtained artificial core samples. A- Artificial core compactor; B- Artificial core mold; C- Artificial core photographs A-E series (C1) and F-G series (C2).

kerogen content, clay mineral content, and crude oil properties. All the cores used in the physical simulation experiments were artificially prepared by the Percolation Physics Laboratory of China University of Petroleum at Beijing (Fig. 6A). The artificial cores are made of quartz sand (grain size <0.25 μm) and epoxy resin. When preparing the cores, the relative ratio of the content of these two raw materials should be determined first, generally 12:1, and evenly placed into the mold (Fig. 6B). Then different variables are considered, including different porosity and permeability, different types and contents of clay minerals, crude oils with different viscosity, and different kerogen contents. After that, all the materials are mixed and evenly distributed in the mold, and the mold is put into the three-axis press, which slowly rises from zero pressure to the design value, and keeps the pressure for 5 h, and the pressure is slowly lowered to zero to stop the operation of the press. Finally, 48 h after core solidification, the mold is removed, cubic core modules with a side length of about 7 cm are taken out, and 2–3 artificial cores with a diameter of 2.50 ± 0.03 cm and a length of 5.00 ± 0.04 cm are taken out of the modules (Fig. 6C). A total of 38 artificial cores were prepared in this study. According to the four main controlling factors in the experimental scheme, these artificial cores were divided into four groups. In group 1, the variable factors were porosity and permeability, and six artificial cores (A1-A6) were prepared under different pressure conditions (10 MPa, 20 MPa, 30 MPa, 40 MPa, 50 MPa, and 60 MPa). In the second group, the variable factors are the types of clay minerals (illite, kaolinite, chlorite, and montmorillonite) and their contents. Under the premise of the pressure being 20 MPa and the ratio of quartz sand to the epoxy resin being unchanged, the single type of clay minerals with the content ratios of 3%, 6%, 9%, 12%, and 15% were added uniformly respectively. The artificial cores with illite as a variable were numbered B1-B5, and there were five cores in total; the artificial cores with kaolinite as a variable were numbered C1-C5, and there were five cores in total; the artificial cores with chlorite as variable are D1-D5, a total of 5 cores; the artificial cores with montmorillonite as a variable were E1-E3, a total of 3 cores. In the third group, the variable factor is the crude oil viscosity, and the parameters set in the preparation of this type of core are the same and consistent with A3 (F1-F8). The variable factor was kerogen content in the fourth group, which was prepared based on shale samples from the Sha-3 member in the Gaoliu area, Nanpu Sag. Under the premise that the pressure is 20 MPa and the ratio of quartz sand and epoxy resin is unchanged, kerogen (G1-G6) with the content ratios of 0%, 3%, 6%, 9%, 12%, and 15% is added evenly. The basic physical properties of all cores were measured by gas measurement

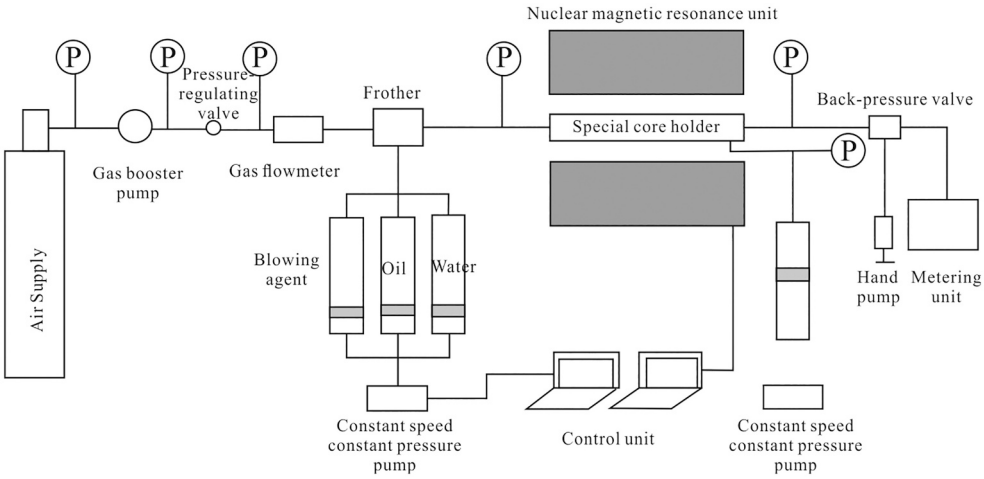

Fig. 7. Nuclear magnetic resonance displacement system and its flow chart for shale oil dynamic study.

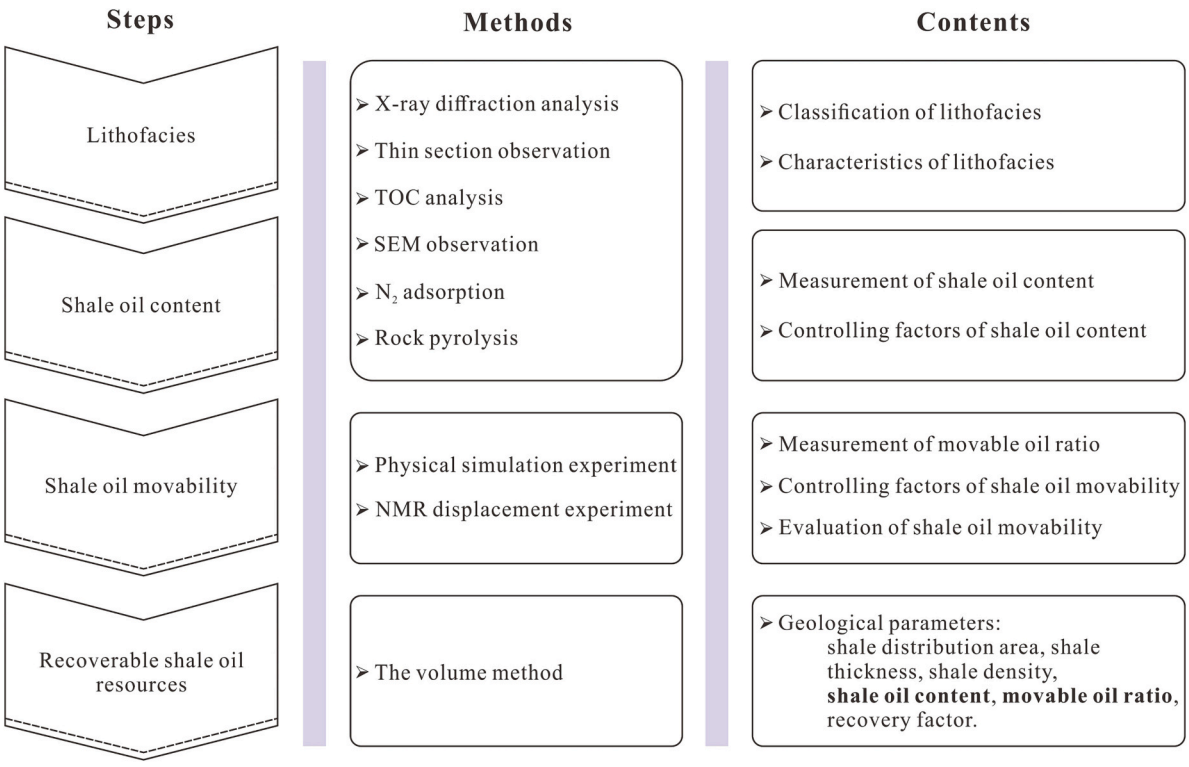

Fig. 8. Technical ideas and workflow of research on shale oil retention and movability evaluation.

before the experiment.

4.3.2. Process of the simulation experiment

The physical simulation experiment of nuclear magnetic displacement was completed in Suzhou Taiyu Testing Co., LTD. The testing process is shown in Fig. 7. The detection instrument was MESOMR23-60H-I Nuclear Magnetic Resonance (NMR) imaging analyzer with a resonance frequency of 23 MHz, a magnetic intensity of 0.5 T, and a magnetic temperature of 32 ± 0.01 °C. The test temperature was 24.5 °C, and humidity was 45.9%. The test was completed in seven steps: The first step is to conduct preliminary treatment for the core. The core cutter is used to cut the experimental core to about 60 mm. After grinding the end, the core length, diameter, and other basic parameters are measured. The second step is to test the core porosity and permeability data. The core is dried for 24 h at 105 °C and put into the core porosity and permeability tester to test the core porosity and permeability. In the third step, the sample was saturated with manganese chloride solution and vacuumed with manganese chloride solution (mass concentration 50%) for eight hours using a vacuum saturation device. In the fourth step, the sample was saturated with crude oil and injected into the crude oil at a flow rate of 0.1 mL/min. The saturated oil cores were placed in white oil and left standing. F1-F8 series artificial cores were saturated with 5#, 6#, 7#, 8#, 9#, 10#, 12#, and 15# crude oil, respectively. The fifth step is to debug NMR parameters. Using NMR analysis application software, the center frequency, pulse width, TW time, and other equipment parameters are tested using standard samples and water film standard samples. The nuclear magnetic resonance (NMR) test was carried out on the rock sample at the sixth step. After the core was placed into the gripper, T2 spectrum cumulative NMR sampling test was carried out to test the T2 spectrum of the core after saturated oil. At the seventh step, the core recovery factor was calculated. Manganese chloride solution (50% mass concentration) was injected at the flow rate of 0.1 mL/min, and 2 MPa followed the confining pressure. After water flooding to 98% water, nuclear magnetic resonance test was performed, and the core recovery factor was calculated.

4.4. Workflow

Studies are carried out in four steps (Fig. 8). In the first step, the lithofacies of shales in the Sha-3 member in Nanpu Sag, Bohai Bay Basin was divided based on thin section observation, X-ray diffraction analysis. The characteristics of structure, organic geochemistry and pore structure of different lithofacies are analyzed by TOC analysis, scanning electron microscope (SEM) observation and gas adsorption test. The second step was to determine the shale oil content through rock pyrolysis analysis. The influencing factors of shale oil content are further analyzed. In the third step, the physical simulation experiment that NMR displacement experiments were conduct on artificial cores prepared were carried out to study the main controlling factors on movable oil ratio and establish a quantitative correlation model for movable oil ratio. Finally, the recoverable oil resources of shales in the third member of Shahejie Formation in the Gaoliu area of Nanpu Sag was evaluated according to the shale oil content, movable oil ratio and other parameters obtained from shale analysis, to provide theoretical guidance for shale oil exploration and development in the future.

5. Results and discussion

5.1. Lithofacies types and characteristics of continental shale

Continental shale is mainly developed in the lacustrine basin with rapid face change and has rich bedding structure. The laminated structure is well developed in continental shale, mainly composed of interbedded dark organic-rich clay laminae and gray calcareous or silty laminae. The thickness of single lamination is generally <1 mm, and it is flat and continuous with light and dark colors. Lithofacies refers to rocks or rock assemblages formed in a particular environment and indicate sedimentary processes and environments (Loucks and Ruppel, 2007). The shale with the same lithofacies has the same geochemical

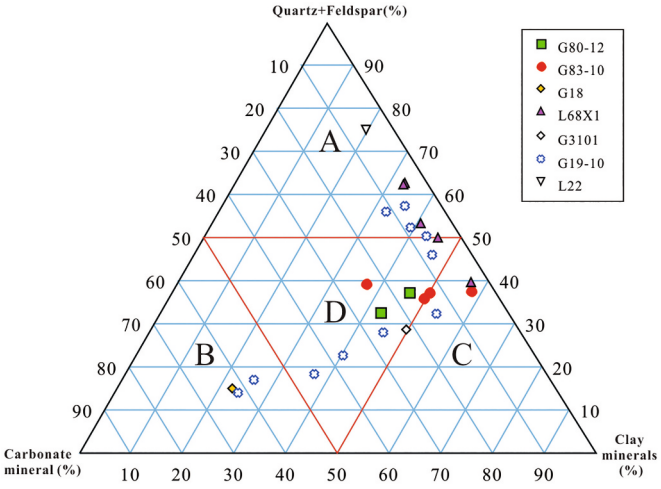

Fig. 9. Triangulation of lithofacies classification of shales in Tertiary Sha-3 member of Nanpu Sag, Bohai Bay Basin (Li et al., 2019b). (A - Siliceous shale; B - Calcareous shale; C - Argillaceous shale; D - Mixed shale).

characteristics, bedding structure, mineral composition, mechanical properties, and oil-gas bearing property (Kale et al., 2010; Aplin and Macquaker, 2011). Many lithofacies classification schemes have been proposed by researchers (Hickey and Henk, 2007; Abouelresh and Slatt, 2011, 2012; Dong et al., 2015). Among these schemes, obtaining mineral composition by XRD analysis is currently the most effective and commonly used lithofacies division scheme (Furmann et al., 2014). Four types of shale lithofacies of the Shahejie Formation in Bohai Bay Basin is divided based on XRD results (Fig. 9). One is siliceous shale with siliceous mineral content ≥50%; The second is calcareous shale with calcium mineral content ≥50%; The third is the argillaceous shale with clay mineral content ≥50%; The fourth is mixed shale with three kinds of mineral contents <50%. Moreover, obvious differences in sedimentary environment, bedding characteristics and organic matter enrichment among the four types of lithofacies can be observed (Fig. 10, Fig. 11). Calcareous shale generally develops in deep lacustrine with highest values of TOC and TS and its organic matter is mainly type I. The relative percentage of organic-rich clay lamina of calcareous shale is >50%. Siliceous and argillaceous shales deposited in shallow lacustrine usually have low TOC and TS values, and type II or III kerogens. The relative percentage of calcareous or silty laminae of siliceous and argillaceous shales is >50%. Mixed shale is developed in the transition zone from shallow to deep lacustrine. TOC and TS values of mixed shale are widely distributed, and gradually increase with the increase of calcium mineral content, and the decrease of siliceous mineral content. With the rise in siliceous mineral content, kerogen type of mixed shale gradually changes from type I to type III.

5.2. *Variation and controlling factors of shale oil content in continental shale*

5.2.1. *Shale oil content*

In this study, the shale oil content was obtained by the pyrolysis method, with light and heavy hydrocarbon calibration comprehensively considered (Eq. (1)). The pyrolysis parameters of shale samples of the Es_3 member before and after dichloromethane extraction in the Dongpu Depression are shown in Table 2. The difference between the pyrolysis parameters S_2 and S_2' is taken as the lost heavy hydrocarbon amount. The light hydrocarbon correction coefficient proposed by Zhu et al. (2015) was used to restore the light hydrocarbon loss. The results show that the S_1 values are in the range of 0.03–12.62 mg/g, with an average of 1.77 mg/g. After light and heavy hydrocarbon calibration, the shale oil content ranges from 0.06 to 32.62 mg/g, with an average of 5.32 mg/g (Table 2).

$$G = \left(S_1 + S_2 - S_2^{'}\right) + (S_1 + S_2)\cdot C_{light} \quad (1)$$

Where G is shale oil content, mg/g; S_1 and S_2 is the pyrolytic parameter of unextracted shale samples, mg/g; S_1' and S_2' is the pyrolytic parameter of shale samples after extracted by dichloromethane, mg/g; C_{light} is the light hydrocarbon calibration coefficient.

5.2.2. *Shale oil content is controlled by lithofaces*

Results show that shale oil content of different lithofacies is different: Calcareous shale has the highest oil content with an average value of

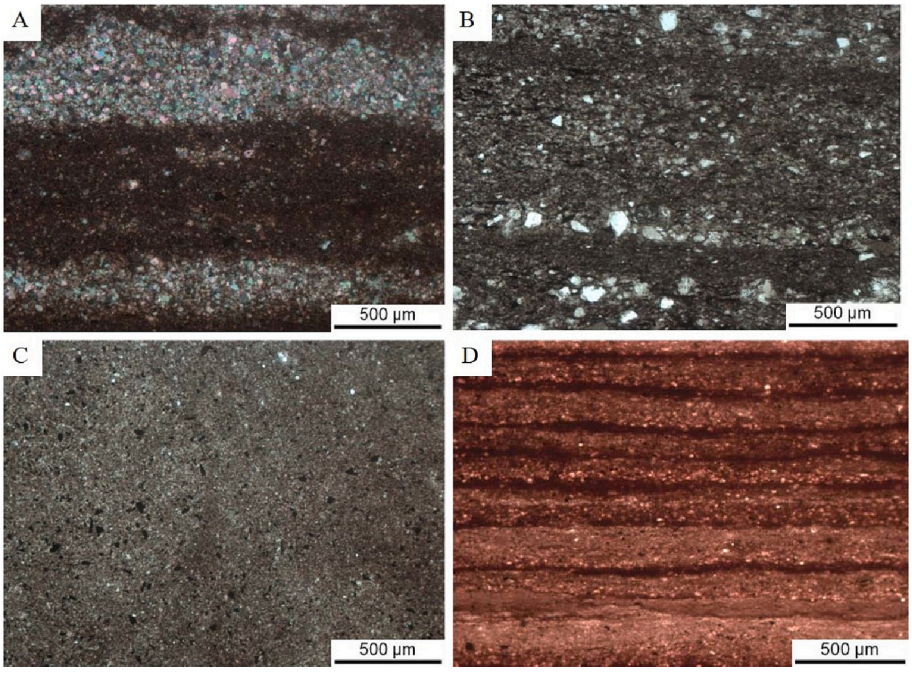

Fig. 10. The shale lithofacies of Sha-3 member in the Nanpu Sag, Bohay Bay Basin, China. A-Calcareous shale; B - Siliceous shale; C-Argillaceous shale; D-Mixed shale.

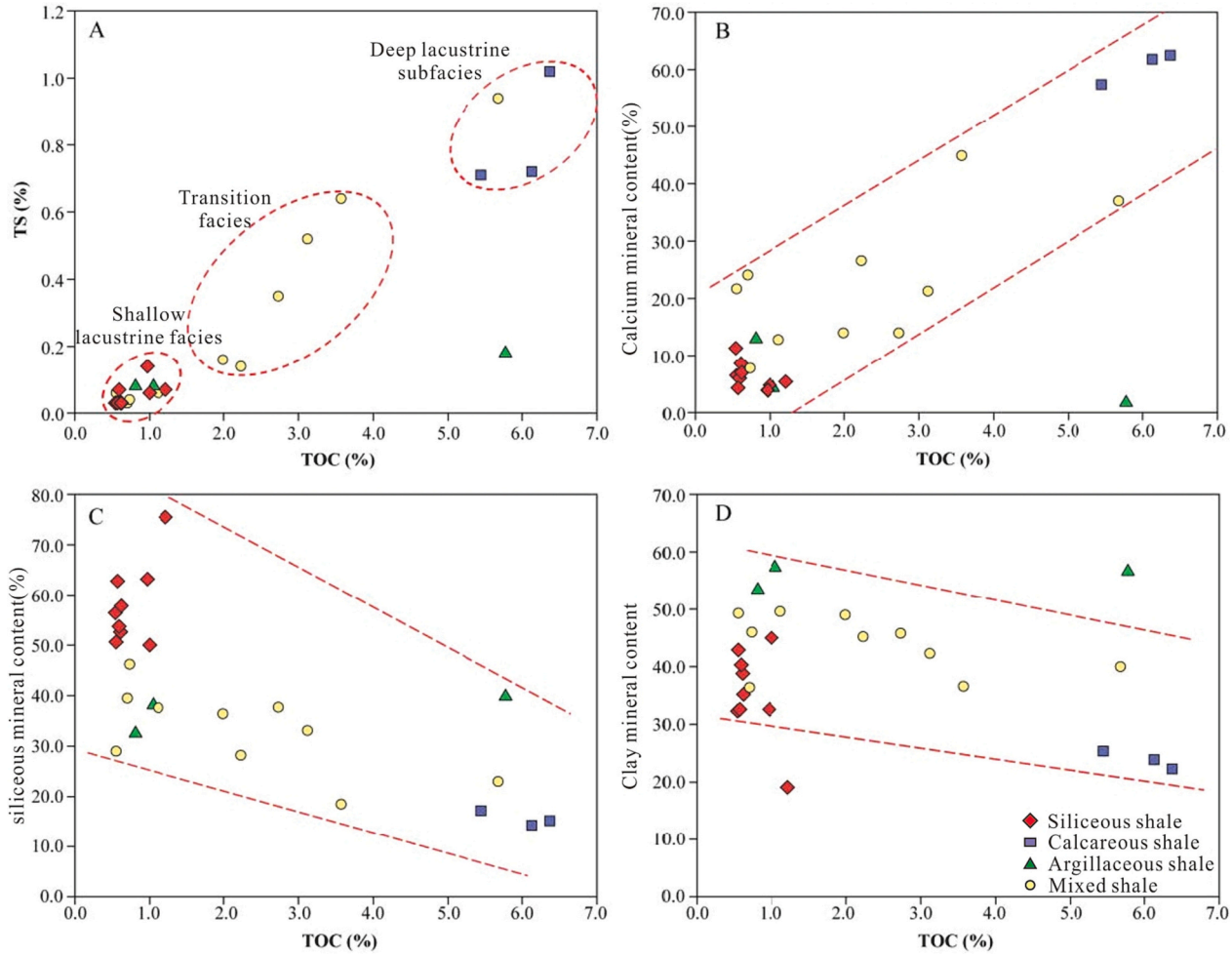

Fig. 11. Sedimentary environment characteristics of different lithofacies shales in the Tertiary Sha-3 member of Nanpu Sag, Bohai Bay Basin (Li et al., 2019b). A-The relationship between TOC and TS; B-The relationship between TOC and calcium mineral content; C-The relationship between TOC and siliceous mineral content; D-Relationship between TOC and clay mineral content.

7.26 mg/g, followed by mixed shale with an average of 5.57 mg/g; the average oil content of argillaceous shale is 4.45 mg/g; siliceous shale has the lowest oil content, averaging 3.54 mg/g (Fig. 12). The controlling effect of lithofaces on shale oil content is manifested in mineral composition, organic matter content and pore structure.

The control of mineral composition on shale oil content is manifested in lithofacies with high clay mineral content, such as argillaceous shale, which is conducive to shale oil enrichment. Compared with matrix minerals such as quartz, feldspar, and carbonates, clay minerals generally have a layered structure and a large specific surface area, enabling hydrocarbon molecules to adsorb on the external surface of clay minerals (Zhao and Zhang, 1990; Wang et al., 2015b). The oil retention capacity of minerals is about 0.20–3.13 mg/g, and the oil retention capacity of clay minerals is greater than that of matrix minerals. The strong ability of clay minerals to retain oil benefits from their lamellar crystal structure and electrical properties. Illite and montmorillonite are composed of two silicon oxide tetrahedral wafers and one aluminum oxide octahedral wafer. Al^{3+} in montmorillonite structure is easily replaced by divalent cations such as Mg^{2+} or Fe^{2+}, whereas Al^{3+} easily replaces Si^{4+} in the structure of illite. Thus, the adsorption capacity of illite to soluble organic matter is greater than that of montmorillonite (Ross and Bustin, 2007).

The abundance and type of organic matter have an important impact on shale oil content. Lithofacies with type I kerogen and high organic matter abundance, such as calcareous shale, are conducive to shale oil enrichment. Organic matter is the source of retained oil in shale, and the retained oil content increases with TOC content of shale (Fig. 13A). The organic-rich lithofacies mainly comes from deep lake to semi-deep lake deposits in saltwater, and planktonic algae mainly supply the organic matter, primarily type I organic matter. The organic matter is structurally composed of many aliphatic chains and a small number of aromatic rings. The organic-poor lithofacies is mainly from shallow lake sediments, mainly type II or type III kerogen. On the one hand, many aliphatic chains of type I kerogen fractured and generated crude oil during thermal evolution, while type III kerogen produced much few liquid hydrocarbons than type I kerogen due to aromatic ring condensation during maturation. On the other hand, due to the structural similarity between crude oil and type I kerogen, the two are more likely to combine in a mutually soluble state. The hydrocarbons can be dissolved in the organic matter in the mud shale. The hydrocarbons with dissolution index similar with that of kerogen are more likely to remain in the kerogen (Ritter, 2003). The pyrolysis S_1 of the extracted samples can reflect the hydrocarbons and organic solvents bound by kerogen in shale. The difference of pyrolysis S_2 of the unextracted samples and extracted samples represents the bound hydrocarbons that cannot be released at 300 °C in shale. Figure13B illustrates the oil retention capacity of different types of kerogen. Compared with the sample containing type II-III kerogen, the oil retention capacity of type I kerogen is stronger.

When considering the control of pore structure on shale oil content, the lithofacies with relatively developed large pores such as calcareous shale is beneficial to the enrichment of shale oil. Different lithofacies

Table 2
Pyrolysis parameters of unextracted and extracted shale samples and shale oil content of the Es_3 shales in the Dongpu Depression (Modified after Shao et al. (2018)).

Number	Well	Depth (m)	Lithofacies	Unextracted shale samples			Extracted shale samples			Ro* (%)	Shale oil content (mg/g)
				S_1 (mg/g)	S_2 (mg/g)	Tmax (°C)	S_1' (mg/g)	S_2' (mg/g)	Tmax' (°C)		
1	Hu82	4216.8	Calcareous shale	0.32	0.8	447	0.04	0.72	450	0.91	32.62
2	Wen210	3848.2	Calcareous shale	1.39	2.27	444	0.05	1.38	446	0.85	2.86
3	Wen75	4226.8	Calcareous shale	2.31	2.22	436	0.03	0.72	443	0.75	0.94
4	Wen210	3778.5	Mixed shale	1.07	1.96	442	0.05	0.89	442	0.80	2.20
5	Hu96	3885.3	Calcareous shale	3.22	8.82	441	0.04	3.83	444	0.80	1.82
6	Wei20	2641.6	Mixed shale	1.18	16.23	431	0.21	12.81	434	0.62	9.95
7	Wen26	2967.5	Calcareous shale	3.92	18.66	435	0.23	13.24	436	0.68	3.24
8	Wei79–1	3349.8	Calcareous shale	1.89	13.49	440	0.14	9.35	440	0.76	2.07
9	Hu7–18	2120.8	Argillaceous shale	0.43	12.42	435	0.24	10.76	436	0.68	1.31
10	Wei42	3277.0	Argillaceous shale	0.09	0.48	437	0.05	0.43	435	0.69	0.06
11	Hu83	4187.0	Siliceous shale	1.25	0.89	421	0.18	0.39	438	0.57	0.48
12	Hu12–20	1777.7	Argillaceous shale	12.62	33.23	434	0.78	13.59	432	0.63	5.62
13	Hu83	4318.3	Mixed shale	0.03	0.12	440	0.06	0.14	435	0.71	3.25
14	Wen75	4215.3	Argillaceous shale	2.94	7.8	447	0.13	5.62	450	0.91	5.72
15	PS18	4076.6	Argillaceous shale	0.24	0.26	454	0.08	0.23	449	0.97	9.54
16	Hu96	4040.6	Siliceous shale	0.49	1.47	445	0.06	0.98	444	0.84	4.20
17	Wen200–6	3729.4	Mixed shale	2.05	2.22	443	0.07	1.04	446	0.84	5.97
18	PS12	4588.8	Siliceous shale	0.07	0.11	461	0.02	0.11	459	1.12	4.67
19	Wei42	3461.7	Siliceous shale	1.04	18.05	444	0.14	14.3	445	0.84	3.96
20	PS4	5193.7	Mixed shale	0.03	0.04	467	0.07	0.05	422	0.84	4.80
21	PS6	4653.0	Argillaceous shale	0.58	1.07	450	0.02	0.62	444	0.89	6.49

* Ro = 0.0180 × Tmax-7.16 (Jarvie et al., 2007).

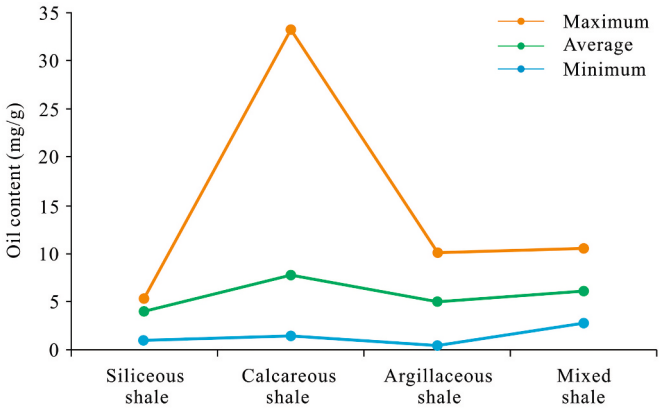

Fig. 12. Comparison of oil contents of four shale lithofacies based on pyrolysis methods.

have different pore development characteristics (Fig. 14). Combined with SEM observation, by comparing the characteristics of N_2 adsorption-desorption curves and pore structure parameters of shale samples before and after hydrocarbon extraction, the pore space characteristics occupied by shale oil are analyzed, and the control of pore structure on shale oil is further discussed (Fig. 15). Before hydrocarbon extraction, the pore volume of shale samples is 0.90–2.68 cm^3/100 g (average 1.54 cm^3/100 g), the SSA is 1.52–9.64 m^2/g (average 4.43 m^2/g), and the pore diameter is 6.93–25.19 nm (average 16.68 nm); After hydrocarbon extraction, the pore volume of the shale samples is 0.98–3.33 cm^3/100 g (average 1.94 cm^3/100 g), the SSA is 1.89–13.79 m^2/g (average 7.43 m^2/g), and the pore diameter is 6.09–19.74 nm (average 11.99 nm) (Table 3). Compared with unextracted samples, the pore volume of extracted samples increased to 1.02–2.13 times, the specific surface area increased to 1.21–3.40 times, and the average pore size decreased by 12%–43% (Table 3). The peak amplitude of pore volume distribution curve with pore size <10 nm increases significantly; The peak of pore volume with pore size larger than 10–20 nm moves to the right (Fig. 16). The shale oil content has good correlation with the pore volume difference before and after extraction (Fig. 17A), indicating that the increased pores after extraction are occupied by oil. Both large pores (pore size >10 nm) and small pores (pore size <10 nm) occupied by the oil that can be extracted from are considered as effective oil-bearing pores; whereas the small pores not occupied by the oil are invalid pores. For effective oil-bearing pores, large pores have obvious advantages than small pores. The oil-bearing volume provided by pores with diameter > 10 nm is 2.13–11.91 times that provided by pores with pore diameter < 10 nm (Fig. 17B). The large pore proportion of calcareous shale is highest, followed by mixed shale, and argillaceous shale and siliceous shale have lowest large pore proportion. The contribution of small pores with size <10 nm in argillaceous and mixed shales to residual hydrocarbon storage is greater than that of siliceous shale and calcareous shale. Combined with previous research findings that shale oil primarily exists in pores with diameter below 100 nm, mainly in the range of 3-80 nm (Wang et al., 2019b), it can be inferred that shale oil mainly exists in the pores with diameter in the range of 10–100 nm.

5.2.3. *Shale oil content is controlled by surrounding rock conditions*

The amount of retained hydrocarbon in shale is controlled by the sealing property of the surrounding rock. The behavior of hydrocarbon molecules at the interface between organic-rich shale and organic-poor surrounding rock is influenced by buoyancy, hydrocarbon-generating expansion force, capillary force, and formation pressure. The former two can be used as the driving force for hydrocarbon expulsion from shale. The formation pressure prevents hydrocarbon from entering the surrounding rock, and the capillary force is related to the properties of the surrounding rock. The pore throat radius and sealing property of surrounding rock are the key factors affecting the amount of hydrocarbon retained in shale. When the expansion force of hydrocarbon generation from organic matter and other hydrocarbon expulsion forces are

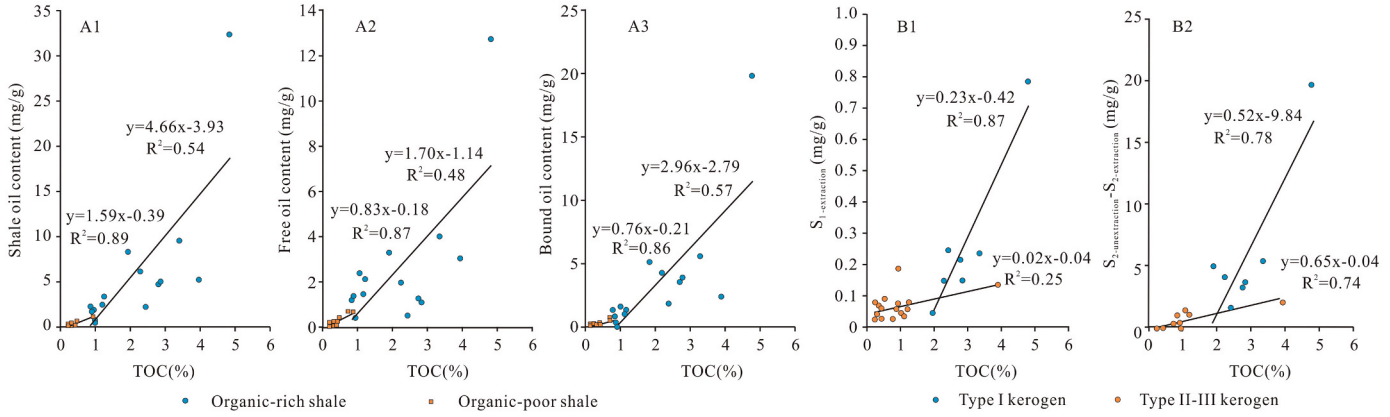

Fig. 13. Correlation between oil retention and organic matter abundance and types of Tertiary Sha-3 shale in Bohai Bay Basin (Modified after Shao et al. (2018)). A1 - The shale oil content is correlated with TOC; A2 - The free oil content of shale is correlated with TOC; A3 - The bound oil content of shale is correlated with TOC; B1 - Correlation between pyrolysis S_1 after extraction and TOC; B2- Pyrolysis S_2 difference before and after extraction is correlated with TOC. The free oil content is approximately treated as the pyrolysis parameter S_1 after light hydrocarbon compensation; The bound oil content approximately equals to pyrolysis S_2 difference before and after extraction. The sum of free oil content and bound oil content equals to shale oil content.

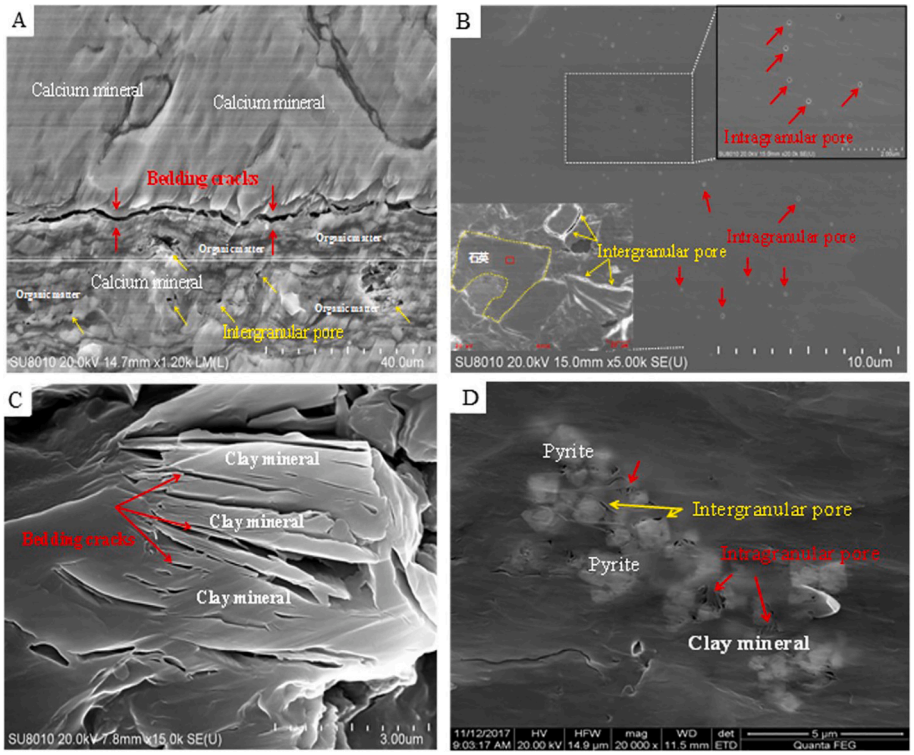

Fig. 14. Pore characteristics in Tertiary Sha-3 shale in Nanpu Sag, Bohai Bay Basin. A- Intergranular pores and microfractures associated with calcareous minerals in calcareous shale; B- Intergranular pores are often developed in quartz and feldspar grains in siliceous shale; C- Clay mineral development interlayer fractures in argillaceous shale; D- Intergranular and intergranular pores in mixed shale.

greater than the capillary resistance of surrounding rock, the remaining hydrocarbons are driven into surrounding rock and the amount of remaining oil in shale decreases; When the hydrocarbon expulsion force is less than the capillary resistance of surrounding rock, the remaining hydrocarbon in shale stays in the source rock, which leads to the increase of shale oil content (Jarvie, 2012).

The test results of hydrocarbon retention in continental shale are related to surrounding rock. The shales of the Sha-3 member in Dongpu Sag, Bohai Bay Basin are mostly thin-bedded and adjacent to salt rock, siltstone, argillaceous siltstone, or silty mudstone in space. Cap rocks with different lithologies have different pore throat radius, so they have different sealing capacity. In this study, the developed and undeveloped areas of salt rock in Dongpu depression are taken as examples to compare and discuss the sealing capacities of gypsum salt rock and mudstone. Statistics on the oil content of 2057 shale samples from 156 wells in salt-bearing and salt-free zones showed that the average pyrolysis hydrocarbon S_1 amount was 0.37–0.45 mg/g in the salt-bearing zone and was 0.02–0.10 mg/g in the salt-free zone (Fig. 18A). Fig. 18B and Fig. 18C respectively show the comparison of the characteristics of chloroform asphalt "A" and hydrocarbon components in the salt-bearing and salt-free mud shale. It is found that the content of saturated hydrocarbon in salt-bearing shale is higher than that in non-salt-bearing shale. In comparison, the content of non-hydrocarbon and asphaltene components is higher in non-salt-bearing shale. These results indicate

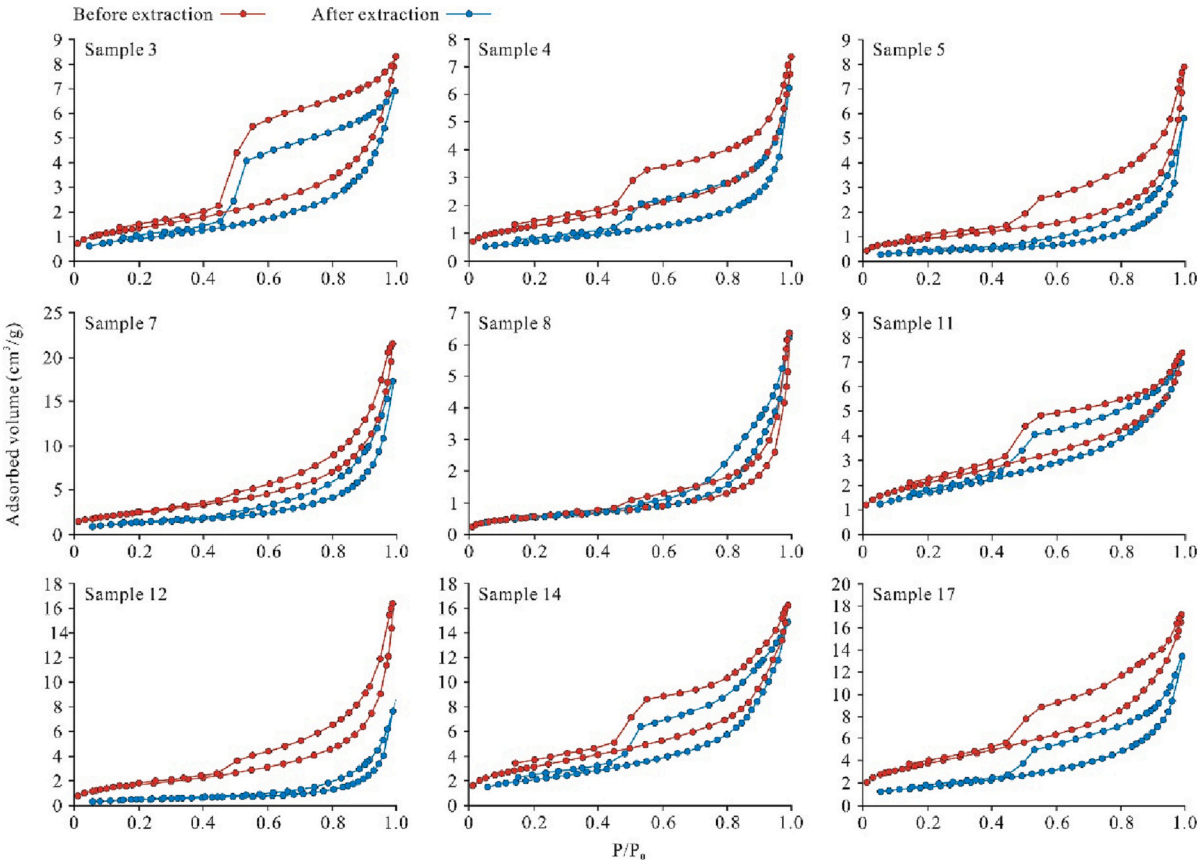

Fig. 15. Comparison of N_2 adsorption-desorption curves between extracted and unextracted shale samples from the Tertiary Sha-3 member in Dongpu Sag, Bohai Bay Basin (Sample numbers, sources and characteristics are shown in Table 3) (Modified after Shao et al. (2018)).

Table 3
Pore structure parameters of unextracted and extracted samples of the Sha-3 member in the Dongpu Sag, Bohai Bay Basin, the locations of wells are illustrated in Fig. 5B.

Sample number	Lithofaces	Unextracted sample			Extracted sample			Pore volume difference before and after extraction (cm^3/100 g)
		Pore volume (cm^3/100 g)	Specific surface area (m^2/g)	Pore size (nm)	Pore volume (cm^3/100 g)	Specific surface area (m^2/g)	Pore size (nm)	
3	Calcareous shale	1.07	3.44	12.42	1.29	4.93	10.43	0.22
4	Mixed shale	0.96	2.54	15.18	1.14	4.59	9.92	0.18
5	Calcareous shale	0.90	1.52	23.74	1.22	3.41	14.33	0.32
7	Calcareous shale	2.68	4.98	21.52	3.33	8.90	14.97	0.65
8	Calcareous shale	0.96	1.96	19.68	0.98	1.89	19.74	0.02
11	Siliceous shale	1.67	9.64	6.93	1.77	11.66	6.09	0.10
12	Argillaceous shale	1.19	1.89	25.19	2.54	6.42	15.85	1.35
14	Argillaceous shale	2.31	7.70	11.98	2.50	11.26	8.87	0.19
17	Mixed shale	2.08	6.17	13.48	2.66	13.79	7.72	0.58

that the retained hydrocarbon amount in shale in the salt-bearing zone is much higher than that in the salt-free zone. Salt rock, as the surrounding rock with good sealing property, leads to the increase of the retained hydrocarbon amount in source rocks.

5.2.4. Shale oil content is controlled by burial depth

The residual hydrocarbon content of shale shows a "big belly" curve distribution with the change of burial depth. Taking the Sha-3 member in Dongpu Sag, Bohai Bay Basin as an example, with the effect of organic matter abundance on the retained hydrocarbon having been removed, the retained hydrocarbon amount of shale increases with the increase of depth above 4000 m and decreases with the rise of depth below 4000 m, presenting a "big belly" curve distribution (Fig. 19A). The hydrocarbon retention amount by per unit organic matter in effective source rocks in six representative basins in China also shows the same variation characteristics with burial depth: Before Ro $\leq$ 1.0%, the retained hydrocarbon amount increases with the increase of burial depth, the maximum value reaches its peak in the period of Ro $\approx$ 1.0%–1.3%; After Ro $\geq$ 1.3%, the retained hydrocarbon amount decreases with the increase of burial depth, and to approaches 0% at Ro $\approx$ 3.5% (Shao et al., 2020b) (Fig. 19B).

The variation of retained hydrocarbon in shale with burial depth is

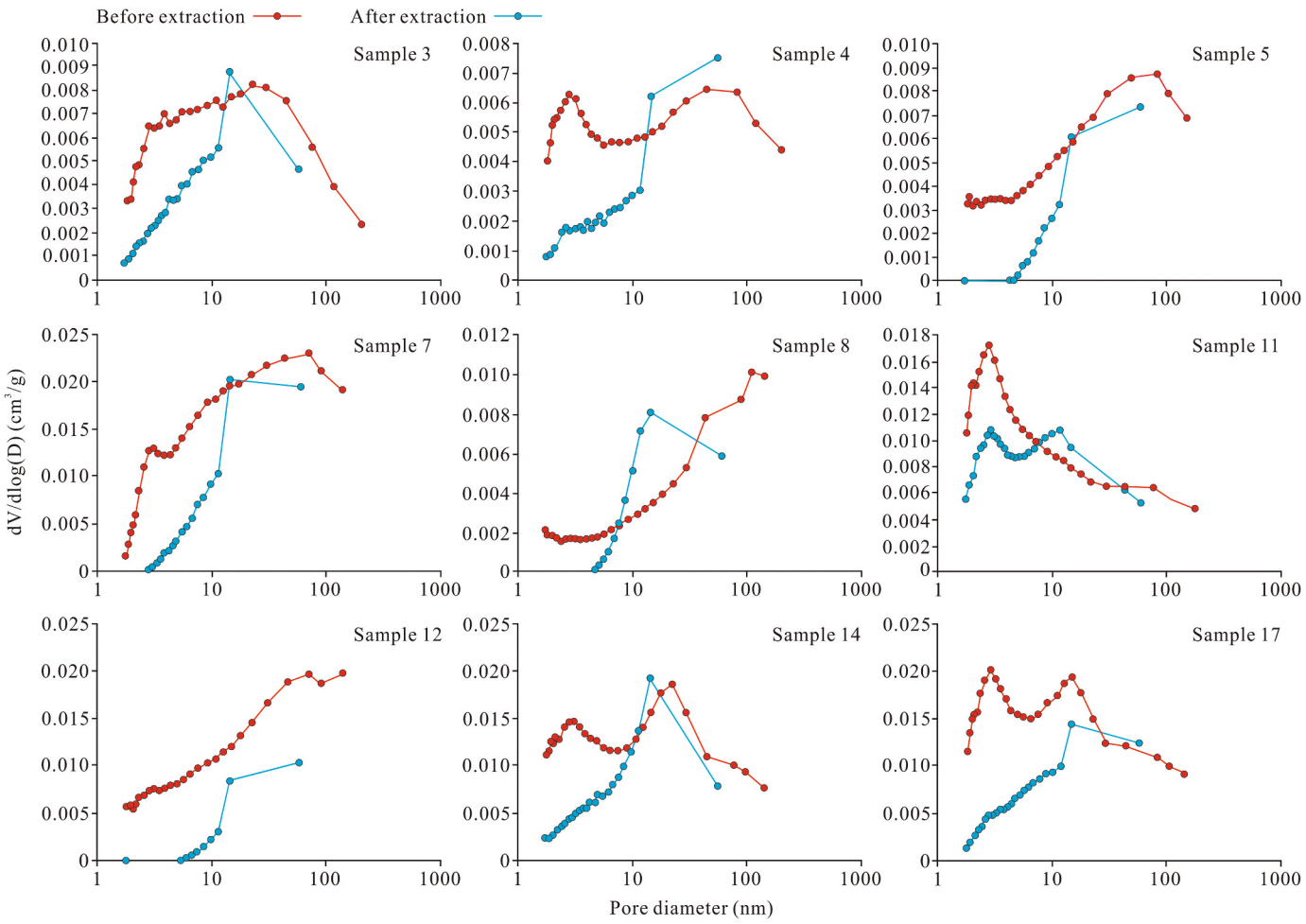

Fig. 16. Comparison of pore size distribution curves between extracted and unextracted shale samples in the Tertiary Sha-3 member of Bohai Bay Basin (Sample numbers, sources and characteristics are shown in Table 3) (Modified after Shao et al. (2018)).

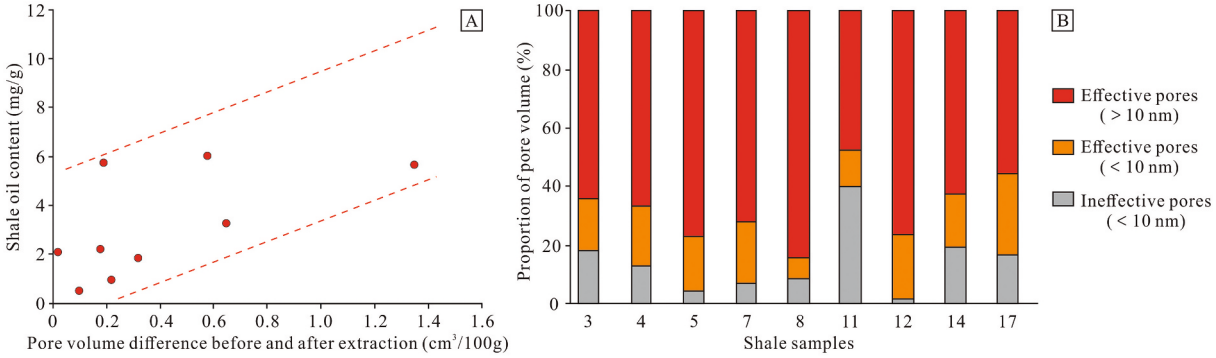

Fig. 17. Correlation between oil retention and pore structure of Tertiary Sha-3 shale of Dongpu Sag, Bohai Bay Basin. A- Relationship between shle oil content and pore volume difference before and after extraction; B- Pore volume structure and composition of shale. Volumn of effective pores (>10 nm) is the volume difference of pore with diameter > 10 nm before and after extraction; Volumn of effective pores (<10 nm) is the volume difference of pore with diameter < 10 nm before and after extraction; Volumn of ineffective pores (<10 nm) is the volumn of pore with diameter < 10 nm before extraction.

controlled by the hydrocarbon generation potential of organic matter. In the process of burial depth, the amount of residual hydrocarbon changes regularly with the change of hydrocarbon generation potential of organic matter and the process of hydrocarbon generation and expulsion (Fig. 19). Generally, the deep burial and high thermal evolution of source rocks can be divided into five stages: The first stage is the shallow burial and immature stage of organic matter with Ro < 0.5%, and almost all the hydrocarbon generated by shale is retained but the amount is small, and only a tiny amount of hydrocarbon is discharged by diffusion phase (Pang, 1995). The second stage is the early stage of organic matter hypogenesis with Ro = 0.5%–1.2%. The hydrocarbon generation rate of source rocks increases with the increase of maturity, and the retained hydrocarbon amount increases with the increase of burial depth to its oversaturation state. The third stage is the mature stage of organic matter with Ro = 1.0%–1.2%. The retained hydrocarbon amount in source rock gradually reaches saturation and reaches its maximum

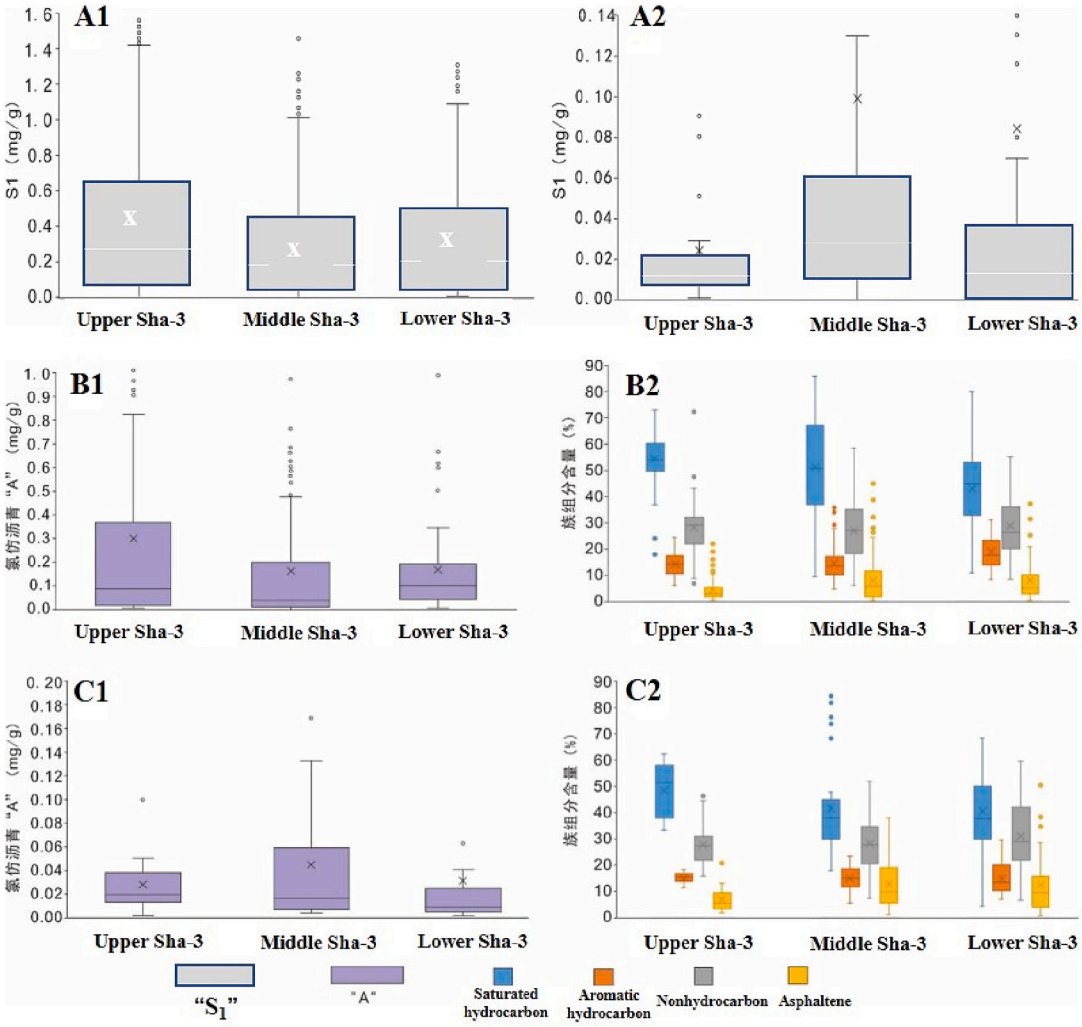

Fig. 18. Correlation between residual oil content of Tertiary shale and surrounding rock in Dongpu Sag, Bohai Bay Basin. A- Comparison of pyrolysis S_1 between salt-bearing area (A1) and salt-free area (A2) of shales in the Sha-3 member; B- Comparison of chloroform bitumen "A" and group composition (B1 and B2) of shale in salt-bearing area; C- characteristics of chloroform bitumen "A" and group components (C1 and C2) of shale in salt-free area.

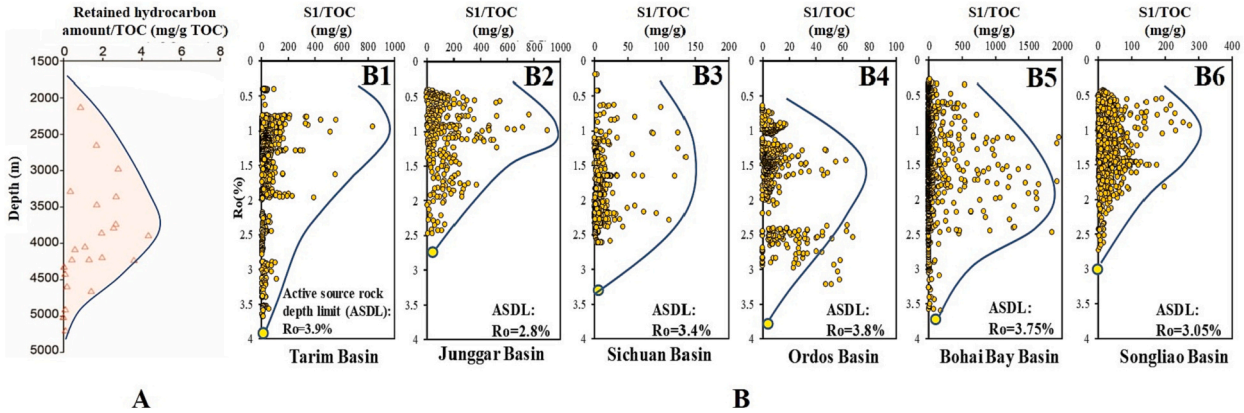

Fig. 19. Variation characteristics of hydrocarbon retention with burial depth of Tertiary shale in Bohai Bay Basin and its comparison with that of source rocks in six representative basins in China. A- The variation characteristics of retained hydrocarbon amount of shale with depth in the Tertiary Sha-3 member in Dongpu Sag. B- Residual hydrocarbon amount of effective source rocks in six representative basins in China: Tarim Basin (B1), Junggar Basin (B2), Sichuan Basin (B3), Ordos Basin (B4), Bohai Bay Basin (B5), Songliao Basin (B6).

value. The fourth stage is the hypogenesis stage or high maturity of organic matter with a Ro = 1.2%–2.0%, liquid hydrocarbon continues to crack, and condensate oil and wet gas are mainly discharged from shale until it all turns into natural gas. Due to the decrease in the hydrocarbon generation potential and the hydrocarbon retention capacity of shales, the retained hydrocarbon amount decreases rapidly. The fifth stage is

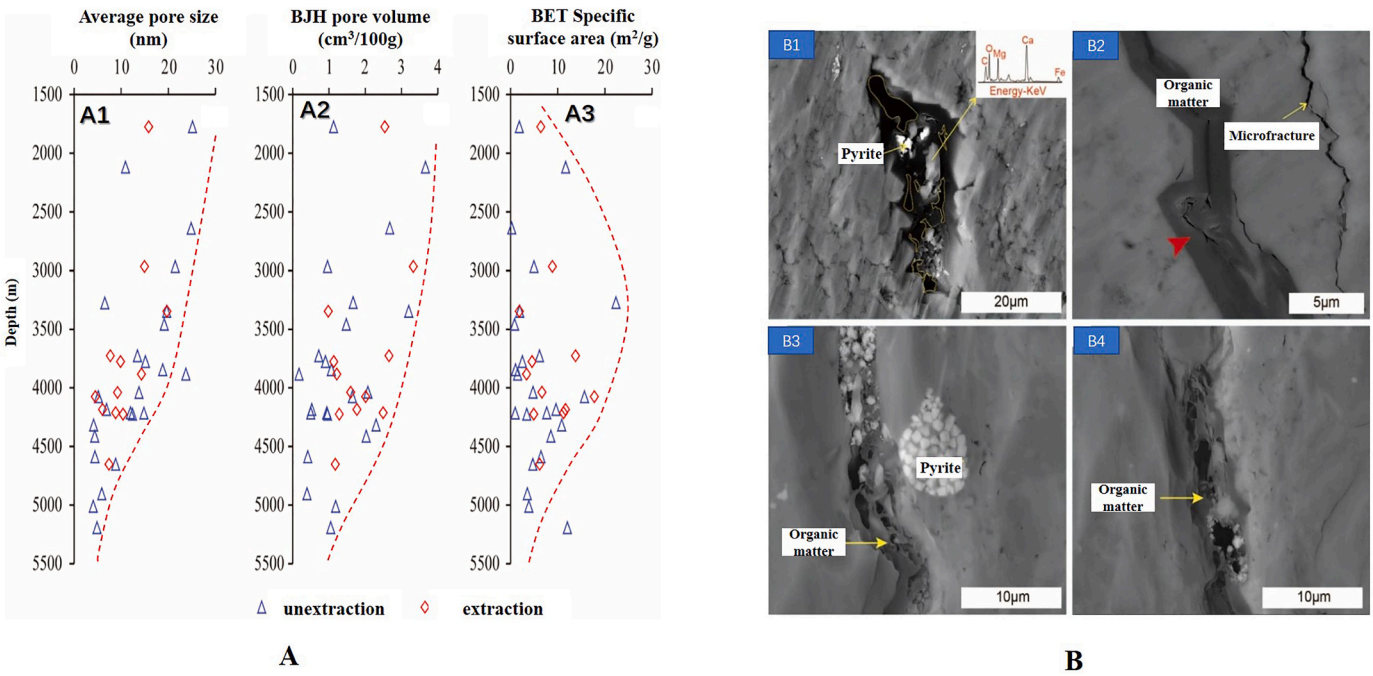

Fig. 20. Variation of shale pore structure with depth and its controlling effect on retained hydrocarbon content of source rocks in the Tertiary Sha-3 member of Dongpu Sag, Bohai Bay Basin (Shao et al. (2018)). A-Shale pore structure changes with depth: A1- Average pore size and depth, A2- Pore volume and depth, A3- Specific surface area and depth; B- Organic pore development characteristics of shale: B1- Primary organic pore (sample 22); B2- Primary organic pore (Sample 3); B3 and B4- Secondary organic pores (Sample 12).

equivalent to organic metamorphism or over-maturity stage with Ro > 2.0%, and almost all liquid oil in shale disappears. Shale oil is gradually transformed into shale gas until no gas is discharged, indicating the formation of the active source-rock depth limit (Pang et al., 2021).

The adsorption of source rock controls the variation of retained hydrocarbon in shale with burial depth. The increase of burial depth results in the densification of shale and affects its hydrocarbon retention ability. N_2 adsorption-desorption experiments show that the pore volume and average pore size of shale decrease with the increase of burial depth, which leads to the decline in hydrocarbon retention capacity and the reduction of actual hydrocarbon retention (Fig. 20A). For the extracted samples, the pore volume of the 5193.7 m buried sample is 58.50% of that of the 1777.71 m buried sample, and the average pore size is only 31.04% of the latter. The specific surface area was positively correlated with the depth above 4200 m and decreased with the increase of depth below 4200 m, indicating that the densification of shale in the early stage of increasing burial depth was mainly caused by the large pores turning into small pores under the action of compaction. The small pores gradually disappeared under the overburden pressure in the late stage. Compaction with the increase of burial depth is the main reason for enhancing the densification of shale and reducing the amount of retained hydrocarbon (Selley, 1978; Magara, 1980). Moreover, organic matter pores begin to develop at a certain buried depth, which provide storage space for retained hydrocarbons. However, the internal pores of

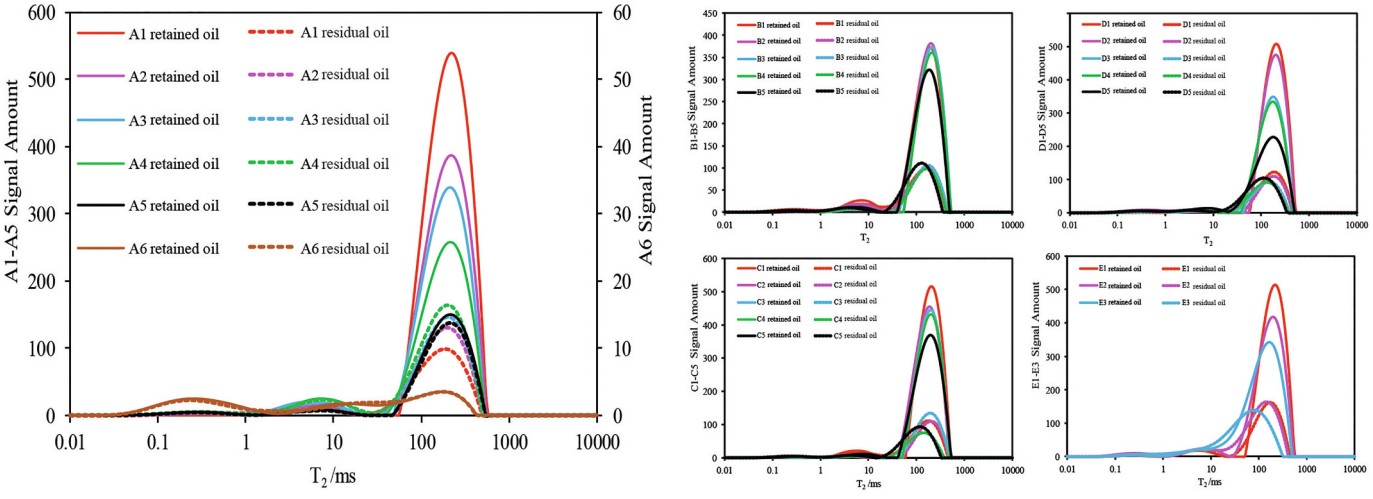

Fig. 21. Moving oil signal variation characteristics and test results of five groups of 24 oil-bearing artificial cores in NMR flooding simulation experiment. The solid line area represents the original retained hydrocarbon amount before the displacement experiment, and the dotted line area represents the residual hydrocarbon amount after the displacement experiment: A- test results of artificial core (A1-A6); B- artificial core test results (B1-B5); C- artificial core test results (C1-C5); D- artificial core test results (D1-D5); *E*- artificial core test results (E1-E3).

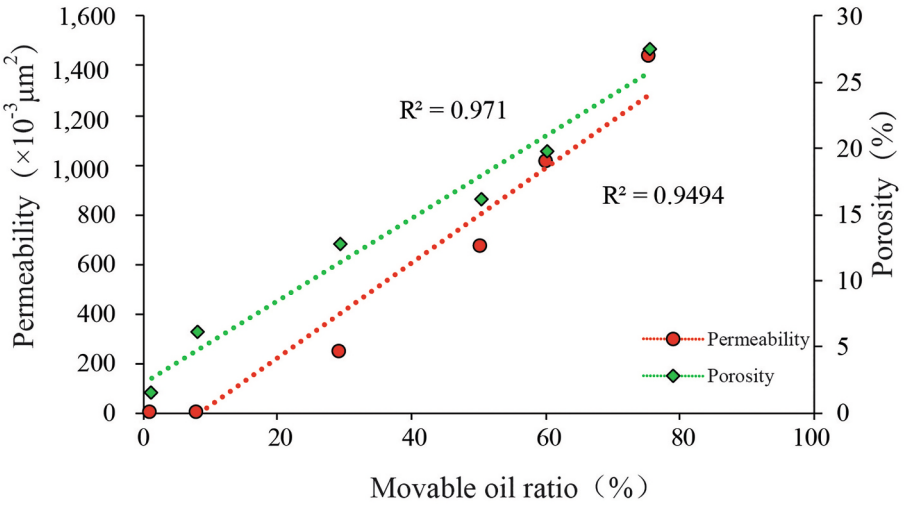

Fig. 22. Variation of movable oil ratio with core permeability in NMR flooding simulation experiment (Group A cores).

organic matter in this study are very rare (Fig. 20B). The organic pores observed by SEM are mainly of primary origin, which is found in lamellar shale, and the single pore diameter is usually larger than 10 μm. Organic matter pores related to thermal evolution are rare in the research area, only found in sample 12, and the burial depth of 4905.01 m has wholly entered the gas generation stage. Organic pores in source rocks of the Sha-3 member in Bohai Bay Basin have little effect on the amount of retained hydrocarbons.

5.3. Main controlling factors and movability evaluation of continental shale oil

5.3.1. Results of physical simulation experiments

The physical simulation experimental results were quantitatively characterized. Fig. 21 shows the comparison of NMR curves and signals of 24 oil-bearing artificial cores in five groups before and after the displacement experiment. The NMR curve of the retained oil in the artificial cores before displacement represents the pore size distribution of the shale sample in the oil-saturated state, which is represented by a solid line. The NMR curve after oil displacement represents the pore size distribution of immovable residual oil, represented by dotted lines. The ratio of the difference between them ($Q_{begin} - Q_{residual}$) and the area enclosed by the abscissa and the original oil-bearing area is the ratio of movable oil ($R_{movable}$). The higher the relaxation time T2 value is, the larger the pore size is; the higher the NMR signal amount is, the larger the pore volume is, and the higher the oil content is. The T2 spectrum curve of the core generally has the characteristics of doublet type, and the relaxation time range of the main peak and the secondary peak is 50–500 ms and 1–20 ms, respectively, indicating that these artificial cores mainly develop two types of pore size. The crude oil is mainly charged in a relatively large pore size range, and the content is very low in a small pore size range. After displacement, the content of crude oil in the larger pore size decreases obviously. In comparison, the content of crude oil in the smaller pore size does not change significantly, indicating that the smaller of pores, the less of retained oil. The relationship between the movable and immovable oil ratios in shale samples and curve signals and the correlation between them is expressed by Eqs. (2)–(4).

$$R_{\text{movable}} = \left(Q_{begin} - Q_{residual}\right)/Q_{begin} \quad (2)$$

$$R_{\text{immovable}} = Q_{remain}/Q_{begin} \quad (3)$$

$$R_{\text{movable}} + R_{\text{immovable}} = 1 \quad (4)$$

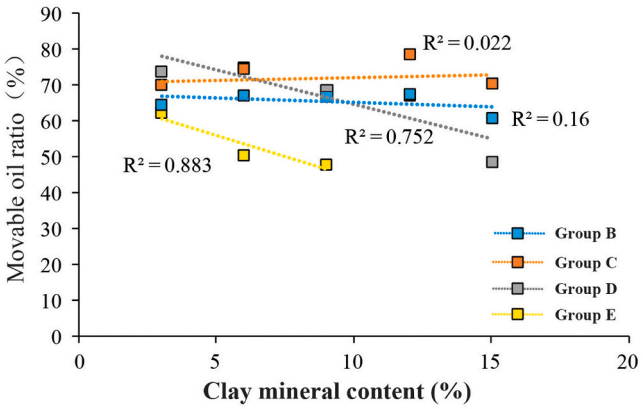

Fig. 23. Variation characteristics of movable oil ratio with clay mineral content and type in NMR displacement physical simulation experiment. Cores of Group B and C contain illite and kaolinite, and cores of Group D and E contain chlorite and montmorillonite, respectively.

5.3.2. Porosity and permeability control movable oil ratio

In the simulation experiment of, Group A-G, the movable oil ratio of core samples (A1-A6) in Group A changed the most, from 75.63% to 1.21% (Fig. 22). The corresponding porosity decreased from 27.49% to 1.54%, and the permeability decreased from 1432.77 × 10^{-3} μm^2 to 0.0022 × 10^{-3} μm^2. The movable oil ratio is positively correlated with core porosity and permeability, and the correlation coefficients are R^2 = 0.971 and R^2 = 0.950, respectively as in Fig. 22. The experimental results clearly show that the better the porosity and permeability of shale is, the higher the movable oil ratio is, and the more favorable it is to development and utilization.

5.3.3. The type and content of clay minerals control movable oil ratio

With the increase of clay mineral content, the ratio of movable oil in shale decreases, and different clay minerals have different effects on the ratio (Fig. 23). The movable oil ratio of core samples containing illite in Group B has the slightest variation, mainly distributed between 60.65% and 67.60%, with an average of 65.34%; The ratio of movable oil in core samples containing kaolinite in Group C ranges from 66.74% to 78.46%, with an average of 72.02%. The correlation between movable oil ratio and clay mineral content is weak, R^2 = 0.16 for Group B and R^2 = 0.022 for Group C, respectively, indicating that illite and kaolinite content have weak adsorption to movable oil. The movable oil ratio in Group D

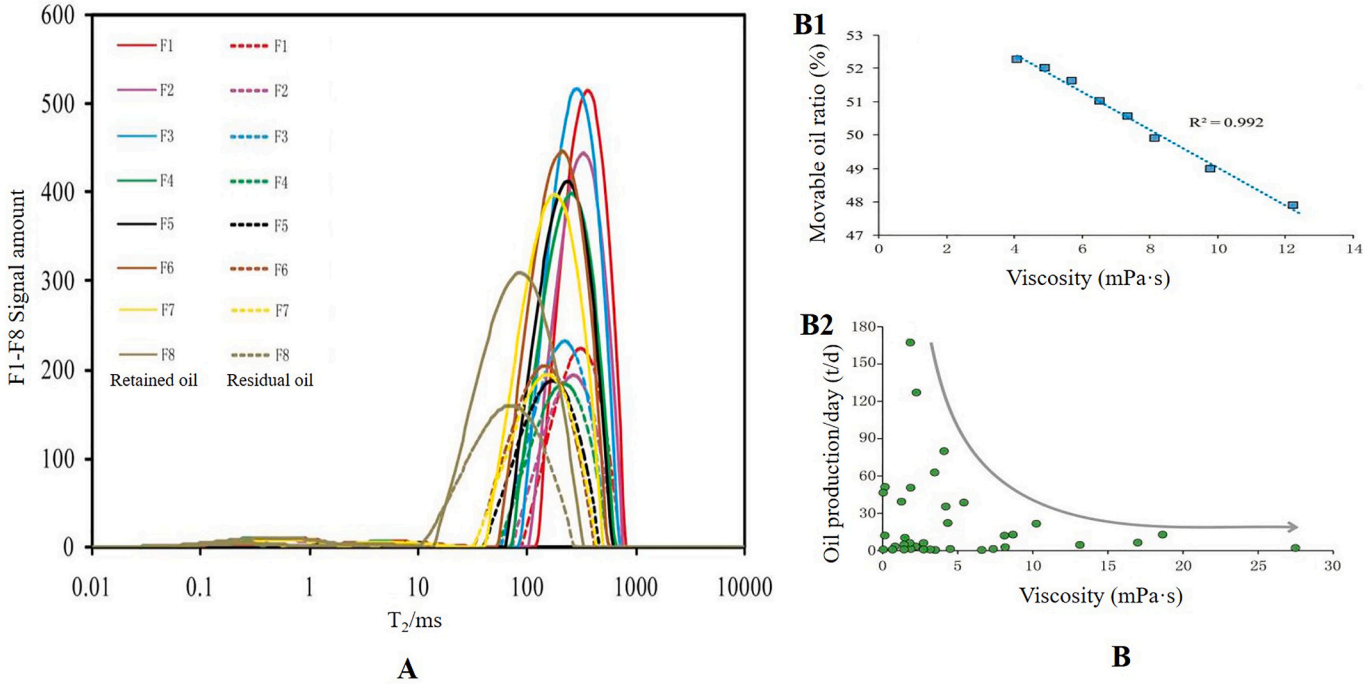

Fig. 24. Variation characteristics of movable oil ratio in rock samples with different crude oil viscosity under physical simulation experimental conditions. A- Movable oil signal changes of core F Group in NMR displacement simulation experiment (core F1-F8); Movable oil ratio changes with crude oil viscosity: B1- NMR flooding simulation results (F1-F8 core), B2- Relationship between crude oil viscosity and shale oil daily production in the Jiyang Depression, Bohai Bay Basin (Ning et al., 2017).

ranged from 48.70% to 74.79%, with an average of 66.51%. The ratio of movable oil in Group E ranged from 47.92% to 62.14%, with an average of 53.54%. The correlation between movable oil ratio and clay mineral content is $R^2 = 0.752$ for Group D and $R^2 = 0.883$ for Group E, respectively. The movable oil ratio decreases with the increase of clay mineral content, which indicates that montmorillonite and chlorite have an inhibitory effect on the movability of crude oil. The specific surface area of the pores in clay minerals are large, but the pore size is small, and the oil and gas mainly exist in an adsorption state, which is not conducive to the flow of oil and gas. The T_2 spectrum before and after displacement shows that the higher the content of clay minerals is, the lower the ratio of movable oil is. The influence of four clay minerals on the movability of crude oil is montmorillonite ≥ chlorite > kaolinite > illite.

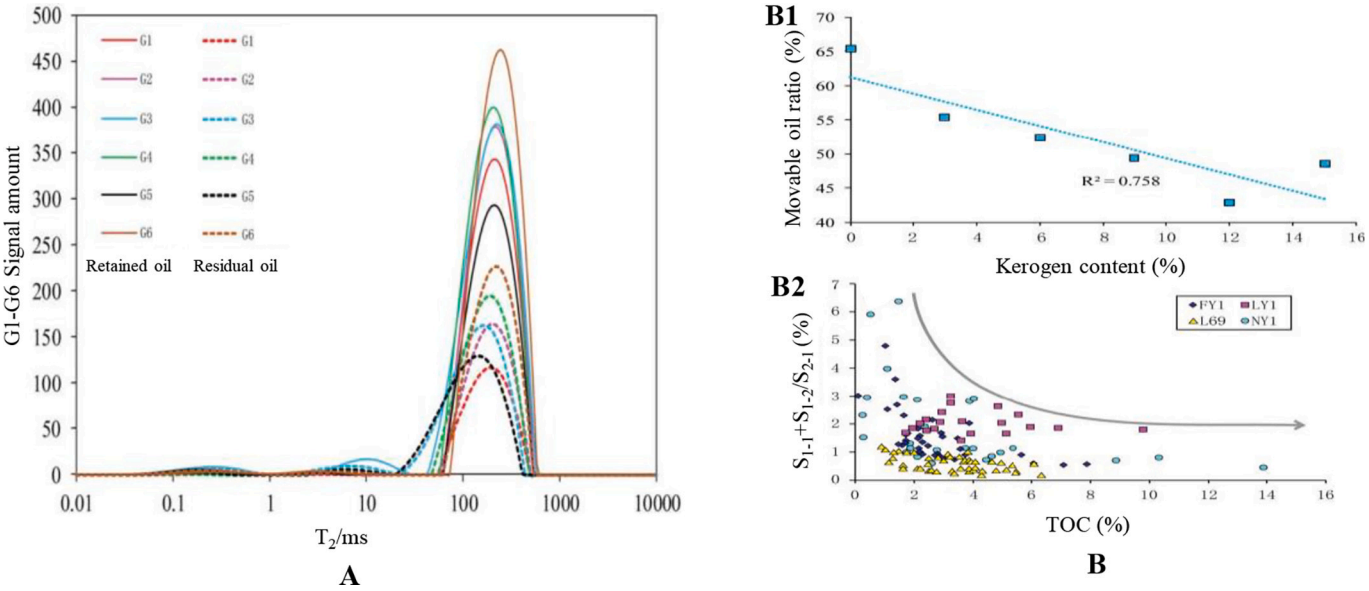

Fig. 25. Variation characteristics of movable oil ratio in shale with kerogen content in NMR displacement simulation experiment. A- Variation characteristics of movable oil signal of Group Cores (G1-G6); B- Movable oil ratio varies with kerogen content: B1- Results of Group G simulation experiment (G1-G6), B2- Results of Rock-Eval pyrolysis of Tertiary shale samples in Bohai Bay Basin (Li et al., 2017), $S_{1-1} + S_{1-2}/S_{2-1}$ is the ratio of movable oil to adsorbed oil. FY1 is Well Fanye 1; LY1 is Liye 1 well; L69 is Luo 69 well; NY1 is Niuye1 well.

Table 4
Associated parameters of Tertiary Sha-3 member shales in the Gaoliu area of Nanpu Sag.

Sample	Y_{actual} (%)	Porosity X_1 (%)	Montmorillonite content X_2 (%)	Organic matter content X_3 (%)	Y_{theory} (%)	Error (%)
G19–10-12	57.14	6.35	13.32	0.54	56.74	−0.40
G19–10-16	64.00	10.48	14.30	0.61	57.29	−6.71
L68X1–6	75.00	4.96	11.45	0.59	58.77	−16.23
L68X1–7	57.14	4.66	14.04	1.00	54.78	−2.36
L68X1–17	85.71	7.66	5.62	0.57	68.53	−17.18
L68X1–4	65.00	7.02	4.32	0.97	70.01	5.01
G19–10-10	50.00	5.36	11.97	0.62	58.20	8.20
G83–10-5	62.20	12.32	7.35	1.99	67.93	5.73
G83–10-7	80.00	4.16	3.35	0.70	70.11	−9.89
G83–10-6	58.70	4.92	7.32	1.12	64.62	5.92
G19–10-9	52.38	4.54	14.72	0.73	53.80	1.42
G80–12–10	45.81	3.31	21.41	2.73	43.05	−2.76
G80–12–1	65.06	11.62	10.79	3.12	62.34	−2.72
G19–10-21	55.54	2.88	9.27	2.23	60.56	5.02

5.3.4. Oil viscosity has a controlling effect on movable oil ratio

The simulated experimental results of displacement of crude oil with different viscosity in core samples of Group F are shown as Fig. 24A. The ratio of movable oil in Group F ranged from 47.93% to 52.27%, with an average of 50.56%; The NMR curves of saturated oil and residual oil show a decreasing trend with the increase of crude oil viscosity, indicating that the ratio of movable oil decreases (Fig. 24B1). There are obvious differences in crude oil properties between continental shale oil in China and marine shale oil in North America: The viscosity of north American marine shale oil is relatively light, while that of continental shale oil in China is high in wax content and viscosity, which is an important reason for the high production of shale oil in Jiyang Depression of Bohai Bay Basin in the early stage and the sharp drop in the later stage (Su et al., 2018). The details are shown in Fig. 24B2, indicating that shale oil viscosity can inhibit shale oil movability and thus affect shale oil production. The experimental results only qualitatively reflect the relationship between the viscosity and the movability of crude oil, in actual geological conditions, the viscosity of crude oil varies in a wide range, and the relationship between the viscosity and the movability of crude oil is more complicated due to the influence of temperature, pressure, components, and other conditions.

5.3.5. Kerogen content has a controlling effect on movable oil ratio

Clay minerals and organic matter have a strong adsorption effect on oil and gas because of their large specific surface area. At present, most studies are focused on the comprehensive impact of the two factors on crude oil retention, but the quantitative research of every single factor is weak. Fig. 25A is the T_2 NMR spectrum of retained oil obtained from core (Group G) samples with different kerogen contents in this study, reflecting the distribution characteristics of the movable ratio of crude oil, varying between 42.80% and 65.38%, with an average of 52.31%. In addition, with the increase of kerogen content, the movable oil ratio of core changes regularly before and after displacement (Fig. 25A). The higher the kerogen content, the lower the movable oil ratio, the correlation coefficient $R^2 = 0.758$ (Fig. 25B1). The Rock-Eval pyrolysis results of shale oil samples from four wells in the Jiyang Depression also show similar characteristics (Fig. 25B2). The ratio of movable oil to adsorbed oil decreases with the increase of TOC content, indicating that shale oil mainly exists in the pore space of kerogen by adsorption, which leads to a decrease in the proportion of movable oil (Li et al., 2017).

5.3.6. Shale oil movability evaluation

Based on the physical simulation results, porosity, montmorillonite content, and kerogen content play major roles in controlling the movability of shale oil through stepwise linear regression. Shale porosity is conducive to the movability of crude oil, while high contents of montmorillonite and kerogen inhibit the movability of crude oil. After the correction of measured values, a quantitative correlation model for movable oil ratio was established (Eq. (5)). The distribution characteristics of related parameters are listed in Table 4: The porosity of shale ranges from 2.9% to 12.3%, with an average of 6.5%; the content of montmorillonite in clay minerals ranges from 3.4%–21.4%, with an average of 10.7%; the organic carbon content ranged from 0.5% to 3.1%, with an average of 1.3%; and the ratio of movable oil of shale in the study area is between 47.3% and 69.5%, with an average of 60.5%. And the absolute error between the calculated movable oil ratio and the measured movable oil ratio is <20% (Eq. (6)).

$$Y_{theory} = 0.48X_1 - 1.45X_2 - 0.23X_3 + 73.13 \quad (5)$$

$$Error = \left(Y_{theory} - Y_{actual}\right)/Y_{actual} \cdot 100\% \quad (6)$$

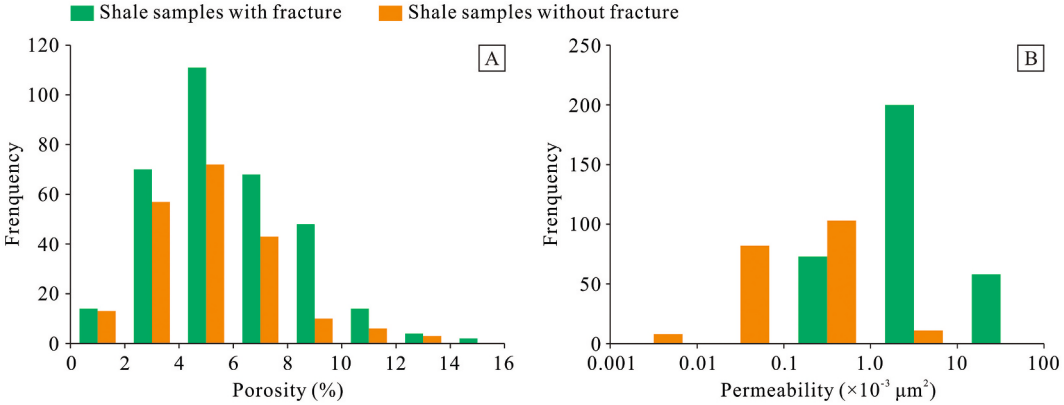

Fig. 26. Distribution characteristics of porosity (A) and permeability (B) of Es_3 shale samples in the Bohai Bay Basin (Data cited from Jiu et al., 2013).

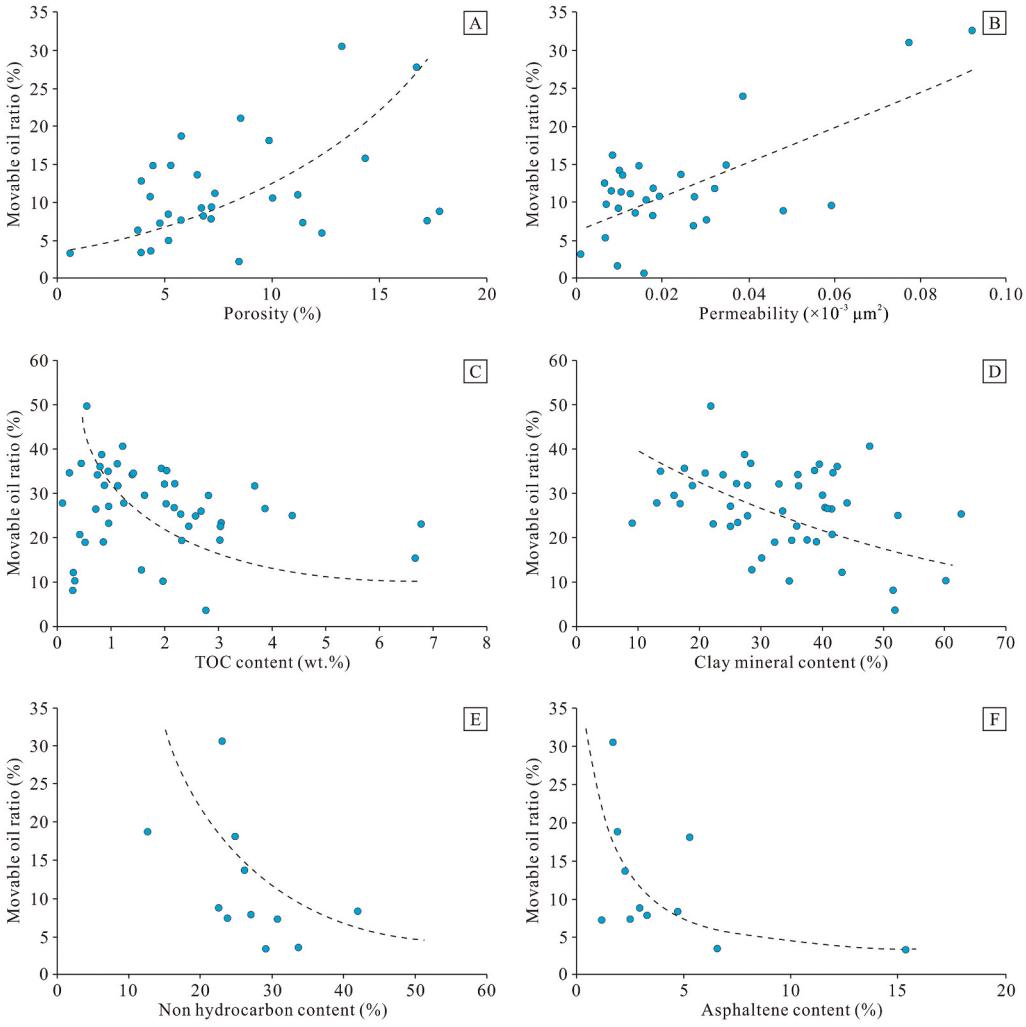

Fig. 27. Relationships between main geological factors and shale oil movability. A- Movable oil ratio vs. porosity (Amended from Guo (2020)); B- Movable oil ratio vs. permeability (Amended from Li et al., 2020); C- Movable oil ratio vs. TOC content (Data cited from Hu et al. (2021)); D- Movable oil ratio vs. clay mineral content (Data cited from Hu et al. (2021)); *E*- Movable oil ratio vs. non hydrocarbon content (Amended from Guo (2020)); F- Movable oil ratio vs. asphaltene content (Amended from Guo (2020)).

In Eq. (6), Y_{theory}—Calculated movable oil ratio of shale, %; Y_{actual}—Measured movable oil ratio of shale, %; X_1– Porosity, %; X_2– Montmorillonite content, %; X_3 – Organic matter content, %.

5.3.7. Comparison with natural shale samples

Statistics show that the porosity and permeability of natural shale samples from the Shahejie Formation in the Bohai Bay Basin are in the range of 0.86%–15.31% (averaging 5.54%) and 0.005×10^{-3}-76.024×10^{-3} μm^2 (averaging 4.794×10^{-3} μm^2), respectively (Fig. 26). The porosity and permeability of shale samples with developed fractures are 1.31%–15.31% (with an average of 5.80%) and 0.161×10^{-3}-76.024×10^{-3} μm^2 (with an average of 7.572×10^{-3} μm^2), respectively. The porosity and permeability of shale samples with undeveloped fractures are 0.86%–13.59% (with a mean of 5.11%) and 0.005×10^{-3}-2.440×10^{-3} μm^2 (with a mean of 0.286×10^{-3} μm^2), respectively. Compared with natural shale samples, the pore structure of artificial cores is relatively simple and their pore size is larger because they have not experienced cementation diagenesis, reflecting the limitations of the application of artificial cores in physical simulation experiments.

The results of this study are compared with those of earlier studies in order to make up for the drawbacks of artificial cores and further confirm the validity of the findings. Previous studies have also been conducted on the controlling factors of shale oil movability. The previous research results also indicated that shale oil movability is influenced by various geological factors such as reservoir characteristics, TOC content, mineral composition, and oil viscosity (Feng et al., 2021). Firstly, the effect of reservoir characteristics including porosity, permeability, and pore structure on shale oil movability is studied. Shale oil is more easily movable the higher the porosity and permeability of the shale (Fig. 27A, B). The pore structure also controls the shale oil movability (Zhang et al., 2022). The larger the specific surface area of small pores, the stronger their adsorption capacity for shale oil. On the other hand, macropores have a smaller specific surface area and a reduced ability to adsorb shale oil (Ning et al., 2020). There is a lower limit of pore size for shale oil's movability, which indicates that flowability only occurs when the pore size exceeds this lower limit (Wang et al., 2015a). The lowest pore size at which shale oil can move, however, is not officially standardized. The lower limit of pore size for shale oil movability, according to Zou et al. (2015b), is 20 nm. According to Bai et al. (2022), the minimum pore size for shale oil movability in the Qingshankou Formation of the Songliao Basin is 10 nm. There is a significant positive correlation between TOC content and movable oil content (Zhao et al., 2021b). Shale oil content and movable oil content both rise in proportion to TOC content. However, as the TOC content rises, the moveable oil ratio falls (Fig. 27C). Shale oil can be strongly absorbed by the surface and pores of kerogen, which prevents the oil from flowing (Lu et al., 2012). Mineral composition also has a significant effect on the movability of shale oil (Li et al., 2019a). Clay minerals have strong adsorption capacity for shale oil due to their large specific surface area (Raji et al., 2015). Quartz and carbonate minerals have poor adsorption capacity for shale oil, and these minerals have strong brittleness, which is conducive to the formation of fractures, increasing the storage space of shale oil, and thus promoting the flow of shale oil (Ougier-Simonin et al., 2016; Zhang et al., 2022). As the content of clay

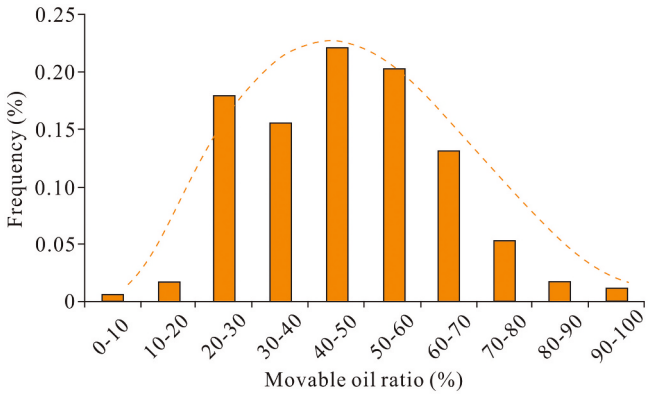

Fig. 28. Statistical analysis results of movable ratio of global shale oil (Li, 2019).

minerals increases, the content of carbonate minerals decreases, and the movable oil ratio decreases (Fig. 27D). In addition, oil viscosity is an important intrinsic factor affecting shale oil movability. The higher the viscosity of shale oil, the worse its movability. The composition of shale oil affects its viscosity. Under certain temperature and pressure conditions, the higher the saturated hydrocarbon content of shale oil and the lower the heavy components such as asphaltene, the lower the viscosity of shale oil and the better its movability (Scheeder et al., 2020). On the contrary, the worse the movability of shale oil (Fig. 27E, F). In summary, the understanding of the main controlling factors of shale oil movability in this study is basically consistent with previous research results.

Moreover, the calculated movable oil ratio values obtained through the physical simulation experiments are not only similar to the measured movable oil ratio values, but also within the normal numerical range of movable oil ratio. The movable oil ratio of 262 unconventional hydrocarbons reservoirs in 12 petroliferous basins obtained by different research methods was statistically analyzed (Fig. 28). It is found that the movable ratio of shale oil in these petroliferous basins is between 3.1%–60.37%, with an average of 27.6%. The movable oil ratio of shale obtained in this paper is within this range, proving the reliability of the results of this study.

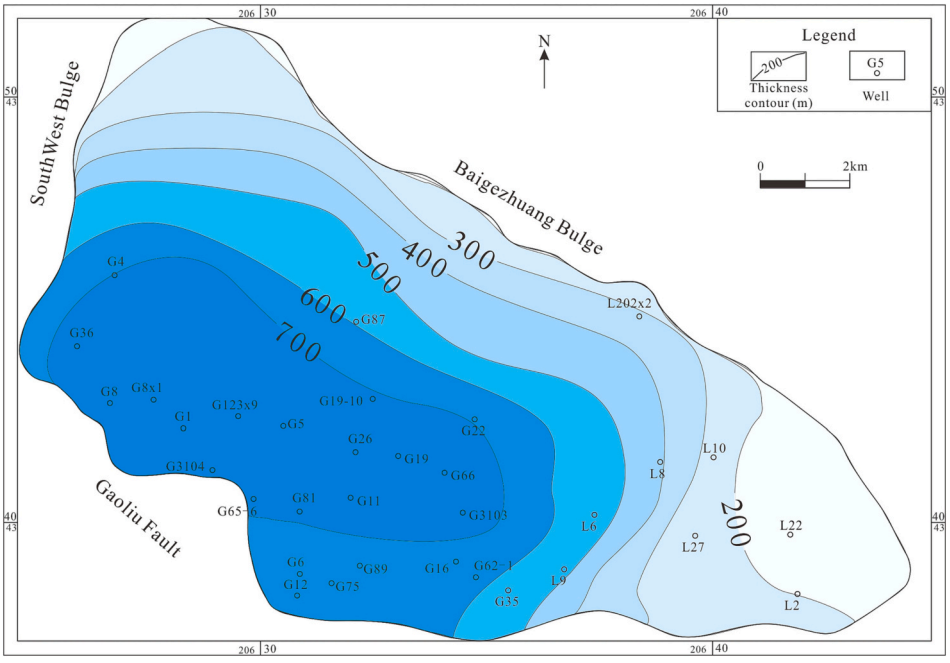

Fig. 29. Shale distribution area (S) and thickness (H) of Tertiary Sha-3 member in the Gaoliu area, Nanpu Sag, Bohai Bay Basin.

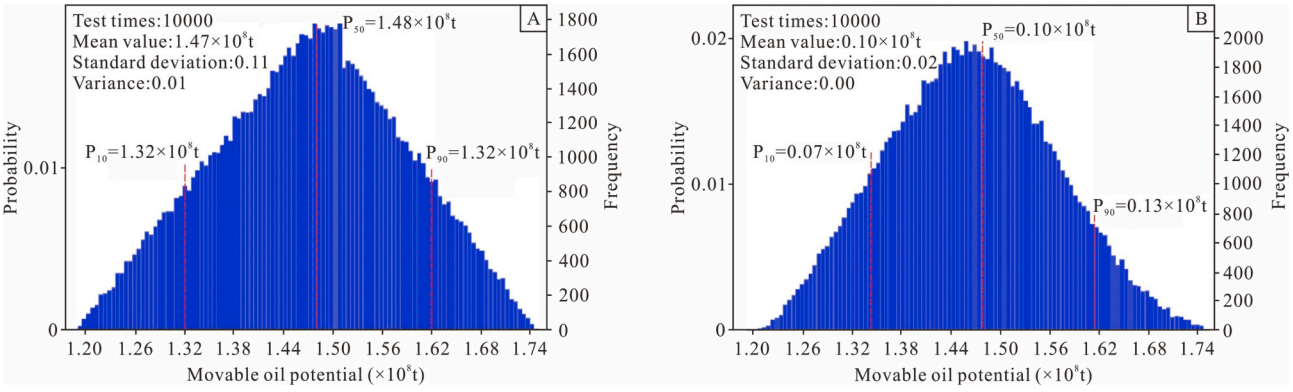

Fig. 30. Monte Carlo simulation results of shale oil resources in the Tertiary Sha-3 member in the Gaoliu area, Nanpu Sag, Bohai Bay Basin: Potential movable shale oil amount (A) and recoverable shale oil resources (B).

5.4. Evaluation of recoverable shale oil resources

5.4.1. Principle of evaluation for potential recoverable resources of shale oil

The exploration and evaluation of continental shale oil resources in China are still in the initial stage (Liu et al., 2014). The volume method is a more suitable method (Wang et al., 2015b). Key geological parameters to be obtained mainly include shale distribution area, thickness, density, oil content, movable oil ratio, and recovery factor (Li et al., 2016; Lu, 2017). The relationship between these six key parameters and the potential recoverable shale oil resources is expressed in Eq. (7):

$$Q = S{\cdot}H{\cdot}D{\cdot}K_r{\cdot}K_m{\cdot}E \quad (7)$$

In Eq. (7), Q – Potential recoverable resources of shale oil, tons; S – Shale oil distribution area, km^2; H– average thickness of shale oil-bearing formations, m; D – Density of shale oil-bearing formations, t/m^3; K_r – average oil content within shale, percentage by weight of rock (%); K_m – movable oil ratio, percentage of the total oil amount in shale (%); E – Shale oil resource recovery factor (%).

5.4.2. Evaluation of shale recoverable oil resources

The volume method evaluates the amount of shale movable oil resources in the Sha-3 member in the Gaoliu area of Nanpu Sag. The values of six key parameters in Eq. (7) are as follows: shale distribution area (S) and thickness (H) shown in Fig. 29; Shale density (D) varied from 2.23 to 2.65 g/cm^3, with an average of 2.45 g/cm^3; The oil content (K_r) of shales of four lithofacies ranged from 1.9% to 20.4%, with an average of 2.5%; Movable oil ratio (K_m) ranged from 47.3% to 69.5%, with an average of 60.5%. The total amount of movable oil and potential recoverable resources of shale in the study area are evaluated by Monte Carlo simulation technology, as shown in Fig. 30. The results show that the movable oil amount corresponds to 1.32×10^8 t and 1.62×10^8 t when the cumulative probability is 10% and 90%, respectively. The movable oil amount is 1.48×10^8 t corresponds to a cumulative probability of 50%. The mode and average values are 1.50×10^8 t and 1.50×10^8 t. The recoverable shale oil resources are 0.07×10^8 t and 0.13×10^8 t, respectively, with the cumulative probability of 10% and 90%, the corresponding results are 0.10×10^8 t with the cumulative probability of 50%. The mode value is 0.095×10^8 t, and the average value is 0.10×10^8 t. The recoverable oil resources in the sweet spot area account for 50% of the total shale oil resources, and their distribution prediction results provide a geological basis for exploration well planning and deployment.

6. Conclusion

(1) There are significant differences between continental shale and marine shale in mineral composition, bedding structure, and lithofacies distribution, which determine the lower movability of continental shale oil than that of marine shale oil.
(2) The continental shale oil content increases with the thinning of sedimentary facies laminae, the increase of internal pore throat radius, and the enhancement of surrounding rock sealing. The retained oil content reaches the maximum when the burial depth is moderate and the thermal evolution degree is Ro ≈ 1.20%.
(3) The physical simulation results of NMR displacement of artificial cores show that the movable oil ratio of shale increases with the increase of porosity and permeability, the decrease of clay mineral content, oil viscosity, and kerogen content.
(4) The obtained parameters such as the shale oil content, movable oil ratio and recovery factor, the volume method and Monte Carlo simulation technology are used to evaluate the recoverable shale oil resources in the Sha-3 member in the Gaoliu area in the range of 950–1000 × 10^4 t.

Declaration of Competing Interest

The authors declare that they have no known competing financial interests or personal relationships that could have appeared to influence the work reported in this paper.

Data availability

The data is in the tables of the manuscript.

Acknowledgments

This study was financially supported by the major science and technology projects of CNPC during the "14th five-year plan" (2021DJ0101), and the Joint Fund of the National Natural Science Foundation of China (U19B6003-02). We thanked Doctor Xinhe Shao in China University of Petroleum (Beijing) for her help in this study. We acknowledged the editors and reviewers for their constructive comments to this manuscript.

Appendix A. Supplementary data

Supplementary data to this article can be found online at https://doi.org/10.1016/j.earscirev.2023.104472.

References

Abouelresh, M.O., Slatt, R.M., 2011. Shale depositional processes: Example from the Paleozoic Barnett Shale, Fort Worth. Cent. Eur. J. Geosci. 3 (4), 398–409. https://doi.org/10.2478/s13533-011-0037-z.
Abouelresh, M.O., Slatt, R.M., 2012. Lithofacies and sequence stratigraphy of the Barnett Shale in east-central Fort Worth Basin Texas. AAPG Bull. 96 (1), 34–43. https://doi.org/10.1306/04261110116.
Abrams, M.A., Thomas, D., 2020. Geochemical evaluation of oil and gas samples from the Upper Devonian and Mississippian reservoirs Southern Anadarko Basin Oklahoma and its implication for the Woodford Shale unconventional play. Mar. Petrol. Geol. 112, 104043 https://doi.org/10.1016/j.marpetgeo.2019.104043.
Altawati, F., Emadi, H., Pathak, S., 2021. Improving oil recovery of Eagle Ford shale samples using cryogenic and cyclic gas injection methods - an experimental study. Fuel 302, 121170. https://doi.org/10.1016/j.fuel.2021.121170.
Aplin, A.C., Macquaker, J.H.S., 2011. Mudstone diversity: Origin and implications for source, seal, and reservoir properties in petroleum systems. AAPG Bull. 95 (12), 2031–2059. https://doi.org/10.1306/03281110162.
Bagri, A., Grantab, R., Medhekar, N.V., Shenoy, V.B., 2010. Stability and formation mechanisms of carbonyl- and hydroxyl-decorated holes in graphene oxide. J. Phys. Chem. C 114, 12053–12061. https://doi.org/10.1021/jp908801c.
Bai, L.H., Liu, B., Du, Y.J., Wang, B.Y., Tian, S.S., Wang, L., Xue, Z.Q., 2022. Distribution characteristics and oil movability thresholds in lacustrine shale reservoir: Insights from N2 adsorption experiments on samples prior to and following hydrocarbon extraction. Pet. Sci. 19 (2), 486–497. https://doi.org/10.1016/j.petsci.2021.10.018.
Bao, S.Y., Zhang, L.Y., Zhang, J.G., Li, J.Y., Li, Z., 2016. Factors influencing movability of Paleogene shale oil in Dongying Sag, Bohai Bay Basin (in chinese with English abstract). Oil Gas Geol. 37 (3), 408–414.
Behar, F., Beaumont, V., De, H.L., Penteado, B., 2001. Rock-Eval 6 technology: Performances and developments. Oil Gas Sci. Technol. 56 (2), 111–134. https://doi.org/10.2516/OGST:2001013.
Bordenave, M.L., 1993. Applied Petroleum Geochemistry. Editions Technips, Paris.
Cao, Z., Liu, G.D., Xiang, B.L., Wang, P., Niu, G., Niu, Z.C., Li, C.Z., Wang, C.Y., 2017. Geochemical characteristics of crude oil from a tight oil reservoir in the Lucaogou Formation, Jimusar Sag, Junggar Basin. AAPG Bull. 101 (1), 39–72. https://doi.org/10.1306/05241614182.
Castro, M.A., Clarke, S.M., Inaba, A., Arnold, T., Thomas, R.K., 1998. Competitive adsorption of simple linear alkane mixtures onto graphite. J. Phys. Chem. B 102, 10528–10534. https://doi.org/10.1021/jp982965z.
Chen, J.Q., Pang, X.Q., Pang, H., Chen, Z.H., Jiang, C.Q., 2018. Hydrocarbon evaporative loss evaluation of lacustrine shale oil based on mass balance method: permian Lucaogou Formation in Jimusaer Depression, Junggar Basin. Mar. Petrol. Geol. 91, 422–431. https://doi.org/10.1016/j.marpetgeo.2018.01.021.
Chen, Z.H., Li, M.W., Jiang, C.Q., Qian, M.H., 2019. Shale oil resource potential and its movability assessment: a case study of Upper Devonian Duvernay shale in Western Canada Sedimentary Basin (In chinese with English Abstract). Oil Gas Geol. 40 (3), 459–468.
Chen, Z.H., Li, M.W., Ma, X.X., Cao, T.T., Liu, X.J., Li, Z.M., Jiang, Q.G., Wu, S.Q., 2018. Generation kinetics based method for correcting effects of migrated oil on Rock-Eval data–An example from the Eocene Qianjiang Formation, Jianghan Basin, China. Int. J. Coal Geol. 195, 84–101. https://doi.org/10.1016/j.coal.2018.05.010.
Cheng, Y.S., Chen, S.L., 2015. Evaluation of Paleozoic Carbonate Reservoirs around Nanpu Sag, Bohai Bay Basin (in Chinese). Central South University Press, Changsha.

Dong, T., Harris, N.B., Ayranci, K., Twemlow, C.E., Nassichuk, B.R., 2015. Porosity characteristics of the Devonian Horn River shale, Canada: Insights from lithofacies classification and shale composition. Int. J. Coal Geol. 141–142, 74–90. https://doi.org/10.1016/j.coal.2015.03.001.
Dong, X.H., Xu, W.J., Liu, R.J., Chen, Z.X., Lu, N., Guo, W.T., 2022. Insights into adsorption and diffusion behavior of shale oil in slit nanopores: a molecular dynamics simulation study. J. Mol. Liq. 359, 119322.
EIA, 2011. International energy outlook. https://www.eia.gov/outlooks/ieo.
EIA, 2012. Annual energy outlook 2013. https://www.eia.gov/forecasts/aeo.
Ertas, D., Kelemen, S.R., Halsey, T.C., 2006. Petroleum expulsion part 1. Theory of kerogen swelling in multicomponent solvents. Energ. Fuel. 20 (1), 295–300. https://doi.org/10.1021/ef058024k.
Falk, K., Pellenq, R., Ulm, F.J., Coasne, B., 2015. Effect of chain length and pore accessibility on alkane adsorption in kerogen. Energy Fuel 29 (12), 7889–7896. https://doi.org/10.1021/acs.energyfuels.5b02015.
Fathi, E., Akkutlu, I.Y., 2012. Lattice Boltzmann method for simulation of shale gas transport in kerogen. SPE J. 18 (18), 27–37. https://doi.org/10.2118/146821-MS.
Feng, Y., Xiao, X.M., Wang, E.Z., Sun, J., Gao, P., 2021. Oil retention in shales: a review of the mechanism, controls and assessment. Front. Earth Sci. 9, 720839 https://doi.org/10.3389/feart.2021.720839.
Fleury, M., Romero-Sarmiento, M., 2016. Characterization of shales using T1–T2 NMR maps. J. Pet. Sci. Eng. 137, 55–60. https://doi.org/10.1016/j.petrol.2015.11.006.
French, K.L., Birdwell, J.E., Lewan, M.D., 2020. Trends in thermal maturity indicators for the organic sulfur-rich Eagle Ford Shale. Mar. Petrol. Geol. 118, 104459 https://doi.org/10.1016/j.marpetgeo.2020.104459.
Fu, J.H., Guo, W., Li, S.X., Liu, X.Y., Cheng, D.X., Zhou, X.P., 2021. Characteristics and exploration potential of muti-type shale oil in the 7th Member of Yanchang Formation, Ordos Basin (in chinese with English abstract). Nat. Gas Geosci. 32 (12), 1749–1761.
Furmann, A., Mastalerz, M., Schimmelmann, A., Pedersen, P.K., Bish, D., 2014. Relationships between porosity, organic matter, and mineral matter in mature organic-rich marine mudstones of the Belle Fourche and Second White Specks formations in Alberta, Canada. Mar. Petrol. Geol. 54 (6), 65–81. https://doi.org/10.1016/j.marpetgeo.2014.02.020.
Guan, M., Liu, X.P., Jin, Z.J., Lai, J., Liu, J., Sun, B., Liu, T., Hua, Z.X., Xu, W., Shu, H.L., Wang, G.C., Liu, M.C., Luo, Y.F., 2022. Quantitative characterization of various oil contents and spatial distribution in lacustrine shales: Insight from petroleum compositional characteristics derived from programed pyrolysis. Mar. Petrol. Geol. 138, 105522 https://doi.org/10.1016/j.marpetgeo.2021.105522.
Guo, Z.Q., 2020. Evaluation of Shale Oil Movability—A Case Study of Shahejie Formation in Jiyang Depression (in Chinese with English abstract). China University of Petroleum (East China), Tsingtao.
Han, W.Z., Zhao, X.Z., Jin, F.M., Pu, X.G., Chen, S.Y., Mu, L.G., Zhang, W., Shi, Z.N., Wang, H., 2021. Sweet spot evaluation and exploration practice of lacustrine shale oil of the second member of Kongdian Formation in Cangdong sag, Bohai Bay Basin. Petrol. Explor. Dev. 48 (4), 900–910. https://doi.org/10.1016/S1876-3804(21)60075-7.
Han, Y., Mahlstedt, N., Horsfield, B., 2015. The Barnett Shale: Compositional fractionation associated with intraformational petroleum migration, retention, and expulsion. AAPG Bull. 99 (12), 2173–2202. https://doi.org/10.1306/06231514113.
He, Q., 2017. China has the third largest shale oil reserves in the world, and the shale gas production target in 2030 can be achieved (in Chinese). https://www.chinanews.com.cn/jingwei/html/10-12/91991.shtml.
Hemmati-Sarapardeh, A., Khishvand, M., Naseri, A., Mohammadi, A.H., 2013. Toward reservoir oil viscosity correlation. Chem. Eng. Sci. 90, 53–68. https://doi.org/10.1016/j.ces.2012.12.009.
Hickey, J.J., Henk, B., 2007. Lithofacies summary of the Mississippian Barnett shale, Mitchell 2 T.P. Sims well, Wise County, Texas. AAPG Bull. 91 (4), 437–443. https://doi.org/10.1306/12040606053.
Hou, L.H., Ma, W.J., Luo, X., Liu, J.Z., Liu, S.H., Zhao, Z.Y., 2021b. Hydrocarbon generation-retention-expulsion mechanism and shale oil producibility of the permian lucaogou shale in the Junggar Basin as simulated by semi-open pyrolysis experiments. Mar. Petrol. Geol. 125, 104880 https://doi.org/10.1016/j.marpetgeo.2020.104880.
Hou, L.H., Zou, C.N., Yu, Z.C., Luo, X., Wu, S.T., Zhao, Z.Y., Lin, S.H., Yang, Z., Zhang, L.J., Wen, D.W., Cui, J.W., 2021a. Quantitative assessment of the sweet spot in marine shale oil and gas based on geology, engineering, and economics: a case study from the Eagle Ford Shale, USA. Energy Strateg. Rev. 38, 100713 https://doi.org/10.1016/j.esr.2021.100713.
Hou, T.G., 2014. Geodynamics of Bohai Bay Basin (in Chinese). Science Press, Beijing.
Hu, H.Y., Hao, F., Guo, X.S., Yi, J.Z., Shu, Z.G., Bao, H.Y., Zhu, X.Y., 2019. Effect of lithofacies on the pore system of over-mature Longmaxi shale in the Jiaoshiba area, Sichuan Basin, China. Mar. Petrol. Geol. 109, 886–898. https://doi.org/10.1016/j.marpetgeo.2019.06.050.
Hu, S.Y., Li, J.Z., Wang, T.S., Wang, Z.C., Yang, T., Li, X., Hou, L.H., Yuan, X.J., Zhu, R.K., Bai, B., Zhuo, Q.G., 2020. CNPC oil and gas resource potential and exploration target selection (in chinese with English abstract). Petrol. Geol. Exp. 42 (05), 813–823.
Hu, T., Pang, X.Q., Jiang, F.J., Wang, Q.F., Liu, X.H., Wang, Z., Jiang, S., Wu, G.Y., Li, C.J., Xu, T.W., Li, M.W., Yu, J.W., Zhang, C.X., 2021. Movable oil content evaluation of lacustrine organic-rich shales: Methods and a novel quantitative evaluation model. Earth-Sci. Rev. 214, 103545 https://doi.org/10.1016/j.earscirev.2021.103545.
IHS Energy, 2014. http://www.ihs.com/.
Jarvie, D.M., 2012. Shale resource systems for oil and gas: Part 2—Shale-oil resource systems. In: Breyer, J.A. (Ed.), Shale Reservoirs-Giant Resources for the 21st Century. AAPG Mem, vol. 97, pp. 89–119.
Jarvie, D.M., 2014. Components and processes affecting producibility and commerciality of shale resource systems. Geol. Acta 12, 307–325. https://doi.org/10.1344/GeologicaActa2014.12.4.3.
Jarvie, D.M., Daniel, M., 2012. Shale resource systems for oil and gas: Part 1-Shale oil resource systems. In: Breyer, J.A. (Ed.), Shale Reservoirs-Giant Resources for the 21st Century, vol. 97. AAPG Mem, pp. 1–19.
Jarvie, D.M., Hill, R.J., Ruble, T.E., Pollastro, R.M., 2007. Unconventional shale-gas systems: the Mississippian Barnett Shale of north-Central Texas as one model for thermogenic shale-gas assessment. AAPG Bull. 91, 475–499. https://doi.org/10.1306/12190606068.
Jiang, F., Chen, D., Wang, Z., Xu, Z., Chen, J., Liu, Y., Huyan, Y., Liu, Y., 2016. Pore characteristic analysis of a lacustrine shale: a case study in the Ordos Basin, NW China. Mar. Pet. Geol. 73, 554–571. https://doi.org/10.1016/j.marpetgeo.2016.03.026.
Jiang, Q.G., Li, M.W., Qian, M.H., Li, Z.M., Li, Z., Huang, Z.K., Zhang, C.M., Ma, Y.Y., 2016. Quantitative characterization of shale oil in different occurrence states and its application (in chinese with English abstract). Petrol. Geol. Exp. 38 (06), 842–849.
Jin, X., Li, G.X., Meng, S.W., Wang, X.Q., Liu, C., Tao, J.P., Liu, H., 2021. Microscale comprehensive evaluation of continental shale oil recoverability. Petrol. Explor. Dev. 48 (1), 256–268. https://doi.org/10.1016/S1876-3804(21)60021-6.
Jiu, K., Ding, W.L., Huang, W.H., Zhang, Y.Q., Zhao, S., Hu, L.J., 2013. Fractures of lacustrine shale reservoirs, the Zhanhua Depression in the Bohai Bay Basin, eastern China. Mar. Petrol. Geol. 48, 113–123.
Kale, S.V., Rai, C.S., Sondergeld, C.H., 2010. Petrophysical characterization of Barnett shale. In: SPE Unconventional Gas Conference.
Khatibi, S., Ostadhassan, M., Xie, Z.H., et al., 2019. NMR relaxometry a new approach to detect geochemical properties of organic matter in tight shales. Fuel 235, 167–177. https://doi.org/10.1016/j.fuel.2018.07.100.
Lafargue, E., Marquis, F., Pillot, D., 1998. Rock-Eval 6 applications in hydrocarbon exploration, production. And soil contamination studies. Oil Gas Sci. Technol. 53 (4), 421–437. https://doi.org/10.2516/OGST:1998036.
Li, B.Y., 2019. Main Controlling Factors of Shale Oil Movability and Evaluation Methods of Resource Potential - a Case Study of Terrestrial Shale in Bohai Bay Basin. China University of Petroleum, (Beijing), China. Ph.D. Thesis.
Li, J., Wang, S., Lu, S., Zhang, P., Cai, J., Zhao, J., Li, W., 2019a. Microdistribution and movability of water in gas shale: a theoretical and experimental study. Mar. Petrol. Geol. 102, 496–507. https://doi.org/10.1016/j.marpetgeo.2019.01.012.
Li, B.Y., Pang, X.Q., Dong, Y.X., Peng, J.W., Gao, P., Wu, H., Huang, C., Shao, X.H., 2019b. Lithofacies and pore characterization in an argillaceous-siliceous-calcareous shale system: A case study of the Shahejie Formation in Nanpu Sag, Bohai Bay Basin. China. J. Petrol. Sci. Eng. 173, 804–819.
Li, J.B., Jiang, C.Q., Wang, M., Lu, S.F., Chen, Z.H., Chen, G.H., et al., 2020. Adsorbed and free hydrocarbons in unconventional shale reservoir: a new insight from NMR T1–T2 maps. Mar. Petrol. Geol. 116, 104311 https://doi.org/10.1016/j.marpetgeo.2020.104311.
Li, J.J., Wang, W.M., Cao, Q., Shi, Y.L., Yan, X.T., Tian, S.S., 2015. Impact of hydrocarbon expulsion efficiency of continental shale upon shale oil accumulations in eastern China. Mar. Petrol. Geol. 59, 467–479. https://doi.org/10.1016/j.marpetgeo.2014.10.002.
Li, J.Y., 2014. Oil and gas contents and movable oil amounts of shales in 4th member of Shahejia Formation, Lijin Subsag, Dongying Sag (in chinese with English abstract). Petrol. Geol. Exp. 36 (3), 365–369.
Li, M.W., Chen, Z.H., Ma, X.X., Cao, T.T., Li, Z.M., Jiang, Q.G., 2018. A numerical method for calculating total oil yield using a single routine Rock-Eval program: A case study of the Eocene Shahejie Formation in Dongying Depression, Bohai Bay Basin, China. Int. J. Coal Geol. 191, 49–65. https://doi.org/10.1016/j.coal.2018.03.004.
Li, M.W., Ma, X.X., Jin, Z.J., Li, Z.M., Jiang, Q.G., Wu, S.Q., Li, Z., Xu, X.Z., 2022b. Diversity in the lithofacies assemblages of marine and lacustrine shale strata and significance for unconventional petroleum exploration in China (in chinese with English abstract). Oil Gas Geol. 43 (1), 1–25.
Li, T.W., Jiang, Z.X., Xu, C.L., Liu, B., Liu, G.H., Wang, P.F., Li, X., Chen, W.T., Ning, C.X., Wang, Z., 2017. Effect of pore structure on shale oil accumulation in the lower third member of the Shahejie formation, Zhanhua Sag, eastern China: evidence from gas adsorption and nuclear magnetic resonance. Mar. Petrol. Geol. 88, 932–949. https://doi.org/10.1016/j.marpetgeo.2017.09.030.
Li, M.Y., Zhu, R.K., Hu, S.Y., 2022a. Geological characteristics and resource potential of overseas terrestrial shale oil (in Chinese with English abstract). Lithol. Res. 34 (1), 163–174.
Li, Z., Zou, Y.R., Xu, X.Y., Sun, J.N., Li, M.W., Peng, P.A., 2016. Adsorption of mudstone source rock for shale oil-experiments, model and a case study. Org. Geochem. 92, 55–62. https://doi.org/10.1016/j.orggeochem.2015.12.009.
Liang, C., Wu, J., Cao, Y.C., Liu, K.Y., Khan, D., 2022. Storage space development and hydrocarbon occurrence model controlled by lithofacies in the Eocene Jiyang Sub-basin, East China: significance for shale oil reservoir formation. J. Pet. Sci. Eng. 215, 110631.
Liu, B., He, J., Lv, Y.F., Ran, Q.C., Dai, C.L., Li, M., 2014. Parameters and method for shale oil assessment: taking Qinshankou Formation shale oil of Northern Songliao Basin (in Chinese with English abstract). J. Central S. Univ.(Sci. Technol.) 45 (11), 3846–3852.
Lopatin, N.V., Zubairaev, S.L., Kos, I.M., Emets, T.P., Romanov, E.A., Malchikhina, O.V., 2003. Unconventional oil accumulations in the upper Jurassic Bazhenov black shale formation, west Siberian Basin: a self-sourced reservoir system. J. Petrol. Geol. 26 (2), 225–244. https://doi.org/10.1111/j.1747-5457.2003.tb00027.x.

Loucks, R.G., Ruppel, S.C., 2007. Mississippian Barnett shale: Lithofacies and depositional setting of a deep-water shale-gas succession in the Fort Worth Basin, Texas. AAPG Bull. 91 (4), 579–601. https://doi.org/10.1306/11020606059.

Lu, S.F., Huang, W.B., Chen, F.W., Li, J.J., Wang, M., Xue, H.T., Wang, W.M., Cai, X.Y., 2012. Classification and evaluation criteria of shale oil and gas resources: disscussion and application. Petrol. Explor. Dev. 39, 249–256. https://doi.org/10.1016/S1876-3804(12)60042-1.

Lu, S.F., 2017. Evaluation methods of movability of shale oil: A comparison and preliminary application. In: The 7th International Symposium on Oil and Gas Accumulation Mechanism and Oil and Gas Resource Evaluation.

Ma, Y.S., Cai, X.Y., Zhao, P.R., Hu, Z.Q., Liu, H.M., Gao, B., Wang, W.Q., Li, Z.M., Zhang, Z.L., 2022a. Geological characteristics and exploration practices of continental shale oil in China (in chinese with English abstract). Acta Geol. Sin. 96 (1), 155–171.

Ma, X.H., Wang, H.Y., Zhou, S.W., et al., 2020. Insights into NMR response characteristics of shales and its application in shale gas reservoir evaluation. J. Nat. Gas Sci. Eng. 84, 103674 https://doi.org/10.1016/j.jngse.2020.103674.

Ma, C., Zhao, X.Z., Yang, T., Jiang, W.Y., Guo, B.C., Han, G.M., Bi, H.B., Ma, J.Y., Bian, C. S., Zhou, K.J., Zhou, S.Y., Zhu, H.J., 2022b. Mineralogy, organic geochemistry, and microstructural characterization of lacustrine Shahejie Formation, Qikou Sag, Bohai Bay Basin: Contribution to understanding microcosmic storage mechanism of shale oil. J. Pet. Sci. Eng. 209, 109843 https://doi.org/10.1016/j.petrol.2021.109843.

Magara, K., 1980. Comparison of porosity-depth relationships of shale and sandstone. J. Petrol. Geol. 3 (2), 175–185. https://doi.org/10.1111/j.1747-5457.1980.tb00981.x.

Michael, G.E., Packwood, J., Holba, A., 2013. Determination of in-situ hydrocarbon volumes in liquid rich shale plays. In: Unconventional Resources Technology Conference, Denver, Colorado, USA.

Mosher, K., He, J.J., Liu, Y.Y., Rupp, E., Wilcox, J., 2013. Molecular simulation of methane adsorption in micro- and mesoporous carbons with applications to coal and gas shale systems. Int. J. Coal Geol. 109, 36–44. https://doi.org/10.1016/j.coal.2013.01.001.

Ning, C.X., Ma, Z.L., Jiang, Z.X., Su, S.Y., Li, T.W., Zheng, L.J., Wang, G.Z., Li, F.X., 2020. Effect of shale reservoir characteristics on shale oil movability in the Lower Third Member of the Shahejie Formation, Zhanhua Sag. Acta Geol. Sin. (Engl. Ed.) 94 (2), 352–363.

Ning, F.X., Wang, X.J., Hao, X.F., Yang, W.Q., Yin, Y., Ding, J.H., Zhu, D.Y., Zhu, D.S., Zhu, J.J., 2017. Occurrence mechanism of shale oil with different lithofacies in Jiyang depression (in chinese with English abstract). Acta Pet. Sin. 38 (02), 185–195.

Ougier-Simonin, A., Renard, F., Boehm, C., Vidal-Gilbert, S., 2016. Microfracturing and Microporosity in Shales. Earth-Sci. Rev. 162, 198–226. https://doi.org/10.1016/j.earscirev.2016.09.006.

Pang, X.Q., 1995. Theory and Application of Hydrocarbon Expulsion Threshold (in Chinese). Petroleum Industry Press, Beijing.

Pang, X.Q., Hu, T., Larter, S., Jiang, Z.X., Li, M.W., Wu, L.Y., Liu, K.Y., Jiang, S., Wang, W.Y., Hu, Q.H., Zhang, K., Li, Z., Bai, H., 2021. Hydrocarbon accumulation depth limit and implications for potential resources prediction. Gondwana Res. https://doi.org/10.1016/j.gr.2021.10.018.

Passey, Q.R., Bohacs, K.M., Esch, W.L., Klimentidis, R., Sinha, S., 2010. From oil-prone source rock to gas-producing shale reservoir-geologic and petrophysical characterization of unconventional shale-gas reservoirs. SPE 131350. https://doi.org/10.2118/131350-MS.

Pepper, A., Corvi, P., 1995. Simple kinetic models of petroleum formation. Part I: oil and gas generation form Kerogen. Mar. Petrol. Geol. 12 (3), 291–319. https://doi.org/10.1016/0264-8172(95)98381-E.

Qian, M.H., Jiang, Q.G., Li, M.W., Li, Z.M., Liu, P., Ma, Y.Y., Cao, T.T., 2017. Quantitative characterization of extractable organic matter in lacustrine shale with different occurrences (in chinese with English abstract). Pet. Geol. Exp. 39 (2), 278–286.

Raji, M., Gröcke, D.R., Greenwell, H.C., Gluyas, J.G., Cornford, C., 2015. The effect of Interbedding on Shale Reservoir Properties. Mar. Petrol. Geol. 67, 154–169. https://doi.org/10.1016/j.marpetgeo.2015.04.015.

Ritter, U., 2003. Solubility of petroleum compounds in kerogen: Implications for petroleum expulsion. Org. Geochem. 34, 319–326. https://doi.org/10.1016/s0146-6380(02)00245-0.

Ross, D.J.K., Bustin, R.M., 2007. Shale gas potential of the Lower Jurassic Gordondale Member, northeastern British Columbia, Canada. B. Can. Petrol. Geol. 55 (1), 51–75.

Sang, Q., Zhang, S.J., Zhu, C.F., Dong, M.Z., Li, Y.J., 2017. Study on movable fluid of continental shale oil reservoir with NMR technology (in chinese with English abstract). China Sci. pap. 12 (9), 978–983.

Scheeder, G., Weniger, P., Blumenberg, M., 2020. Geochemical Implications from Direct Rock-Eval Pyrolysis of Petroleum. Org. Geochem. 146, 104051 https://doi.org/10.1016/j.orggeochem.2020.104051.

Selley, R.C., 1978. Porosity gradients in North Sea oil-bearing sandstones. J. Geol. Soc. 135 (1), 119–132.

Shao, X.H., Pang, X.Q., Li, H., Hu, T., Xu, T.W., Xu, Y., Li, B.Y., 2018. Pore network characteristics of lacustrine shales in the Dongpu Depression, Bohai Bay Basin, China, with implications for oil retention. Mar. Petrol. Geol. 96, 457–473.

Shao, D.Y., Zhang, T.W., Ko, L.T., Li, Y.F., Yan, J.P., Zhang, L.L., Luo, H., Qiao, B., 2020a. Experimental investigation of oil generation, retention, and expulsion within Type II kerogen-dominated marine shales: Insights from gold-tube nonhydrous pyrolysis of Barnett and Woodford Shales using miniature core plugs. Int. J. Coal Geol. 217, 103337 https://doi.org/10.1016/j.coal.2019.103337.

Shao, X.H., Pang, X.Q., Li, M.W., Li, Z.M., Zhao, Y., 2020b. Hydrocarbon generation from lacustrine shales with retained oil during thermal maturation. Petrol. Sci. 17, 1478–1490. https://doi.org/10.1007/s12182-020-00487-1.

Slatt, R.M., O'Brien, N.R., 2011. Pore types in the Barnett and Woodford gas shales: contribution to understanding gas storage and migration pathways in finegrainedrocks. AAPG Bull. 95 (12), 2017–2030. https://doi.org/10.1306/03301110145.

Smith, J.L., 2018. Estimating the future supply of shale oil: a Bakken case study. Energ. Econ. 69, 395–403. https://doi.org/10.1016/j.eneco.2017.11.026.

Song, Y.T., Liao, Y.S., Zhang, S.C., 2005. Determination of soluble organic matter in two occurrence states in brackish-salt lacustrine source rocks and its significance (in chinese with English abstract). Chin. Sci. Bull. 50 (14), 1531–1534.

Su, S.Y., Jiang, Z.X., Shan, X.L., Zhang, C.W., Zou, Q.T., Li, Z., Zhu, R.F., 2018. The effects of shale pore structure and mineral components on shale oil accumulation in the Zhanhua Sag, Jiyang Depression, Bohai Bay Basin, China. J. Petrol. Sci. Eng. 165, 365–374. https://doi.org/10.1016/j.petrol.2018.02.030.

Sun, S., Zhang, T., 2020. A 6M digital twin for modeling and simulation in subsurface reservoirs. Adv. Geo-Energy Res. 4 (4), 349–351. https://doi.org/10.46690/ager.2020.04.01.

Sun, S.S., Dong, D.Z., Li, Y.P., Wang, H.Y., Shi, Z.S., Huang, S.W., Chang, Y., Bai, W.H., 2021. Geological characteristics and controlling factors of hydrocarbon accumulation in terrestrial shale in the Da'anzhai Member of the Jurassic Ziliujing Formation, Sichuan Basin (in chinese with English abstract). Oil Gas Geol. 42 (1), 124–135.

Tao, Z., He, Z.L., Alves, T.M., Guo, X.W., Gao, J., He, S., Zhao, W., 2022. Structural inheritance and its control on overpressure preservation in mature sedimentary basins (Dongying depression, Bohai Bay Basin, China. Mar. Petrol. Geol. 137, 105504 https://doi.org/10.1016/j.marpetgeo.2021.105504.

Tian, S., Erastova, V., Lu, S., Greenwell, H., Underwood, T.R., Xue, H., Zeng, F., Chen, G., Wu, C., Zhao, R., 2018. Understanding model crude oil component interactions on kaolinite silicate and aluminol surfaces: toward improved understanding of shale oil recovery. Energy Fuel 32, 1155–1165.

Tian, S.S., Xue, H.T., Lu, S.F., Zeng, F., Xue, Q.Z., Chen, G.H., Wu, C.Z., Zhang, S.S., 2017. Molecular simulation of oil mixture adsorption character in shale system. J. Nanosci. Nanotechnol. 17, 6198–6209. https://doi.org/10.1166/jnn.2017.14487.

Wang, X.L., Zhang, G.S., Tang, W., Wang, D.H., Wang, K., Liu, J.Y., Du, D., 2022c. A review of commercial development of continental shale oil in China. Energy Geosci. 3, 282–289. https://doi.org/10.1016/j.engeos.2022.03.006.

Wang, A.Q., Zheng, B.M., 1987. Calibration of analytic parameters for pyrolytic chromatography (in Chinese with English abstract). Exp. Petrol. Geol. 9 (4), 342–350.

Wang, E.Z., Feng, Y., Guo, T.L., Li, M.W., 2022b. Oil content and resource quality evaluation methods for lacustrine shale: a review and a novel three-dimensional quality evaluation model. Earth-Sci. Rev. 239, 121848 https://doi.org/10.1016/j.earscirev.2022.104134.

Wang, E.Z., Li, C.R., Feng, Y., Song, Y.C., Guo, T.L., Li, M.W., Chen, Z.H., 2022a. Novel method for determining the oil movable threshold and an innovative model for evaluating the oil content in shales. Energy 239 (A), 121848. https://doi.org/10.1016/j.energy.2021.121848.

Wang, M., Ma, R., Li, J., Lu, S., Li, C., Guo, Z., Li, Z., 2019. Occurrence mechanism of lacustrine shale oil in the Paleogene Shalehejie formation of Jiyang depression, Bohai Bay basin, China. Petrol. Explor. Dev. 46, 833–846. https://doi.org/10.1016/S1876-3804(19)60242-9.

Wang, S., Feng, Q.H., Javadpour, F., Xia, T., Li, Z., 2015b. Oil adsorption inshale nanopores and its effect on recoverable oil-in-place. Int. J. Coal Geol. 147–148, 9–24. https://doi.org/10.1016/j.coal.2015.06.002.

Wang, S., Feng, Q.H., Zha, M., Lu, S.F., Qin, Y., Xia, T., Zhang, C., 2015a. Molecular dynamic simulation of liquid alkane occurrence state in pores and fractures of shale organic matter. Petrol. Explor. Dev. 42 (06), 772–778. https://doi.org/10.11698/PED.2015.06.10.

Wang, S., Javadpour, F., Feng, Q.H., 2016. Molecular dynamics simulations of oil transport through inorganic nanopores in shale. Fuel 171, 74–86. https://doi.org/10.1016/j.fuel.2015.12.071.

Wang, M., Yang, J.X., Wang, Z.W., Lu, S.F., 2015c. Nanometer-scale pore characteristics of lacustrine shale, Songliao Basin, NE China. PLOS One 10 (8), 1–18. https://doi.org/10.1371/journal.pone.0135252.

Wang, Y., Liu, L.F., Zheng, S.S., Luo, Z.H., Sheng, Y., Wang, X.M., 2019. Full-scale pore structure and its controlling factors of the Wufeng-Longmaxi shale, southern Sichuan Basin, China: Implications for pore evolution of highly overmature marine shale. J. Nat. Gas Sci. Eng. 67, 134–146. https://doi.org/10.1016/j.jngse.2019.04.020.

Wu, X.L., Gao, B., Ye, X., Bian, R.K., Nie, H.K., Lu, F.Z., 2013. Shale oil accumulation conditions and exploration potential of faulted basins in the east of China (in chinese with English abstract). Oil Gas Geol. 34 (4), 455–462.

Xia, S.Q., Lin, C.S., Wu, W., Du, X.F., 2022. Sequence architecture, depositional evolution and responses to tectonic subsidence and lacustrine fluctuation in lacustrine rift basin: a case study from Cenozoic Liaodong Bay, Bohai Bay Basin. J. Pet. Sci. Eng. 208, 109494 https://doi.org/10.1016/j.petrol.2021.109494.

Xu, J., Ji, F.J., 2015. Structure and Evolution of Bohai Bay Basin (in Chinese). Seismological Press, Beijing.

Xu, X.Y., Liu, W.B., Bai, J., Chen, S., Li, Y.H., 2021. Enrichment characteristics and resource potential of shale oil in the first member of Qingshankou Formation in southern Songliao Basin (in Chinese with English abstract). Geol. Resour. 30 (3), 296–305.

Xu, Y., Lun, Z.M., Pan, Z.J., Wang, H.T., Zhou, X., Zhao, C.P., Zhang, D.F., 2022. Occurrence space and state of shale oil: a review. J. Pet. Sci. Eng. 211, 110183 https://doi.org/10.1016/j.petrol.2022.110183.

Xue, H.T., Tian, S.S., Lu, S.F., Zhang, W.H., Du, T.T., Mu, G.D., 2015. Selection and Verification of Key Parameters in the Quantitative Evaluation of Shale Oil: a Case

Study at the Qingshankou Formation, Northern Songliao Basin (in chinese with English abstract). Bull. Mineral. Petrol. Geochem. 34 (01), 70–78+2.
Zeng, P.H., Ye, Z.B., Zhang, X.C., He, Y.L., Wu, Y.X., Lai, N.J., 2023. Molecular dynamics simulation of shale oil adsorption on quartz surface with different wettability (in Chinese with English abstract). J. At. Mol. Phys. 40 (3), 036005.
Zhang, H., Huang, H.P., Li, Z., Liu, M., 2019. Oil physical status in lacustrine shale reservoirs – A case study on Eocene Shahejie Formation shales, Dongying Depression, East China. Fuel 257, 116027. https://doi.org/10.1016/j.fuel.2019.116027.
Zhang, J.C., Lin, L.M., Li, Y.X., Tang, X., Zhu, L.L., Xing, Y.W., Jiang, S.L., Jing, T.Y., Yang, S.Y., 2012. Classification and evaluation of shale oil (in chinese with English abstract). Earth Sci. Front. 19 (5), 322–331.
Zhang, L.Y., Bao, Y.S., Li, J.Y., Li, Z., Zhu, R.F., Zhang, J.G., 2014. Movability of lacustrine shale oil: a case study of Dongying Sag, Jiyang Depression, Bohai Bay Basin. Petrol. Explor. Dev. 41 (6), 703–711. https://doi.org/10.1016/S1876-3804(14)60084-7.
Zhang, P.F., Lu, S.F., Li, J.Q., Chang, X.C., Lin, Z.Z., Chen, G., Li, J.J., Liu, J.Z., Tian, S.S., 2022. Evaluating microdistribution of adsorbed and free oil in a lacustrine shale using nuclear magnetic resonance: a theoretical and experimental study. J. Pet. Sci. Eng. 212, 110208.
Zhang, Y.N., Fang, T.M., Ding, B., Wang, W.D., Yan, Y.G., Li, Z., et al., 2020. Migration of oil/methane mixture in shale inorganic nano-pore throat: a molecular dynamics simulation study. J. Pet. Sci. Eng. 187, 106784 https://doi.org/10.1016/j.petrol.2019.106784.
Zhao, X.Z., Pu, X.G., Zhou, L.H., Jin, F.M., Han, G.M., Shi, Z.N., Han, W.Z., Ding, Y.J., Zhang, W., Wang, G.N., Liu, X.W., Wang, H., 2021a. Enrichment theory, exploration technology and prospects of shale oil in lacustrine facies zone of deep basin: a case study of the Paleogene in Huanghua depression, Bohai Bay Basin (in chinese with English Abstract). Acta Pet. Sin. 42 (2), 143–162.
Zhao, X.Y., Zhang, Y.Y., 1990. Analysis of Clay Minerals and Clay Minerals (in Chinese). China Ocean Press, Beijing.
Zhao, W.Z., Hu, S.Y., Hou, L.H., Yang, T., Li, X., Guo, B.C., Yang, Z., 2020a. Types and resource potential of continental shale oil in China and its boundary with tight oil. Petrol. Explor. Dev. 47 (1), 1–11. https://doi.org/10.1016/S1876-3804(20)60001-5.
Zhao, W.Z., Zhang, B., Wang, X.M., Wu, S.T., Zhang, S.C., Liu, W., Wang, K., Zhao, X., 2021b. Differences in Source Kitchens for Lacustrine In-Source and Out-Source Hydrocarbon Accumulations Onshore China. Petrol. Explor. Dev. 48 (03), 464–475. https://doi.org/10.1016/s1876-3804(21)60044-7.
Zhao, X.Z., Zhou, L.H., Pu, X.G., Jin, F.M., Shi, Z.N., Han, W.Z., Jiang, W.Y., Han, G.M., Zhang, W., Wang, H., Ma, J.Y., 2020b. Formation conditions and enrichment model of retained petroleum in lacustrine shale: A case study of the Paleogene in Huanghua depression, Bohai Bay Basin, China. Petrol. Explor. Dev. 47 (5), 916–930. https://doi.org/10.1016/S1876-3804(20)60106-9.
Zheng, S.J., Yao, Y.B., Liu, D.M., Cai, Y.D., Liu, Y., 2018. Characterizations of full-scale pore size distribution, porosity and permeability of coals: a novel methodology by nuclear magnetic resonance and fractal analysis theory. Int. J. Coal Geol. 196, 148–158. https://doi.org/10.1016/j.coal.2018.07.008.
Zheng, T.Y., Zieger, L., Baniasad, A., Grohmann, S., Hu, T., Littke, R., 2022. The Shahejie Formation in the Dongpu Depression, Bohai Bay Basin, China: Geochemical investigation of the origin, deposition and preservation of organic matter in a saline lacustrine environment during the Middle Eocene. Int. J. Coal Geol. 253, 103967 https://doi.org/10.1016/j.coal.2022.103967.
Zhong, J., Wang, P., Zhang, Y., Yan, Y.G., Hu, S.Q., Zhang, J., 2013. Adsorption mechanism of oil components on water-wet mineral surface: a molecular dynamics simulation study. Energy 59, 295–300. https://doi.org/10.1016/j.energy.2013.07.016.
Zhu, C.F., Guo, W., Li, Y.J., Gong, H.J., Sheng, J.J., Dong, M.Z., 2021. Effect of occurrence states of fluid and pore structures on shale oil movability. Fuel 288, 119847. https://doi.org/10.1016/j.fuel.2020.119847.
Zhu, G., Wang, Z., Su, J., 2013. Geochemical characteristics of high-quality hydrocarbon source rocks in the Nanpu Sag of the Bohai Bay Basin, China. Oil Shale 30 (2), 117–135. https://doi.org/10.3176/oil.2013.2.03.
Zhu, H.J., Ju, Y.W., Huang, C., Han, K., Qi, Y., Shi, M.Y., Yu, K., Feng, H.Y., Li, W.Y., Ju, L.T., Qian, J., 2019. Pore structure variations across structural deformation of Silurian Longmaxi Shale: an example from the Chuandong Thrust-Fold Belt. Fuel 241, 914–932. https://doi.org/10.1016/j.fuel.2018.12.108.
Zhu, R.F., Zhang, L.Y., Li, J.Y., Liu, Q., Li, Z., Wang, R., Zhang, L., 2015. Quantitative evaluation of residual liquid hydrocarbons in shale (In chinese with English Abstract). Acta Pet. Sin. 36 (1), 13–18.
Ziegs, V., Horsfield, B., Skeie, J.E., Rinna, J., 2017. Petroleum retention in the Mandal Formation, Central Graben, Norway. Mar. Petrol. Geol. 83, 195–214. https://doi.org/10.1016/j.marpetgeo.2017.03.005.
Zink, K.G., Scheeder, G., Stueck, H.L., Biermann, S., Blumenberg, M., 2016. Total shale oil inventory from an extended Rock-Eval approach on non-extracted and extracted source rocks from Germany. Int. J. Coal Geol. 163, 186–194. https://doi.org/10.1016/j.coal.2016.06.023.
Zou, C.N., Jin, X., Zhu, R.K., Gong, G.M., Sun, L., Dai, J.X., Meng, D.P., Wang, X.Q., Li, J.M., Wu, S.T., Liu, X.D., Wu, J.T., Jiang, L., 2015b. Do shale pore throats have a threshold diameter for oil storage? Sci. Rep. 5, 13619. https://doi.org/10.1038/srep13619.
Zou, C.N., Yang, Z., Cui, J.W., Zhu, R.K., Hou, L.H., Tao, S.Z., Yuan, X.J., Wu, S.T., Lin, S.H., Wang, L., Bai, B., Yao, J.L., 2013a. Formation mechanism, geological characteristics and development strategy of nonmarine shale oil in China. Petrol. Explor. Dev. 40, 15–27. https://doi.org/10.1016/S1876-3804(13)60002-6.
Zou, C.N., Zhai, G.M., Zhang, G.Y., Wang, H.J., Zhang, G.S., Li, J.Z., Wang, Z.M., Wen, Z.X., Ma, F., Liang, Y.B., Yang, Z., Li, X., Liang, K., 2015a. Formation, distribution, potential and prediction of global conventional and unconventional hydrocarbon resources. Petrol. Explor. Dev. 42 (1), 13–25. https://doi.org/10.1016/S1876-3804(15)60002-7.
Zou, C.N., Zhang, G.S., Yang, Z., Tao, S.Z., Hou, L.H., Zhu, R.K., Yuan, X.J., Ran, Q.Q., Li, D.H., Wang, Z.P., 2013b. Geological concepts, characteristics, resource potential and key techniques of unconventional hydrocarbon: on unconventional petroleum geology. Petrol. Explor. Dev. 40 (04) https://doi.org/10.11698/PED.2013.04.01, 385–399+454.